COO 1109-86

THE SOLID STATE CHEMISTRY OF RARE EARTH OXIDES

LeRoy Eyring

A. Jerome Skarnulis

Richard T. Tuenge

Robert B. Von Dreele

APPROVED:

____
LeRoy Eyring, Principal Investigator

____
Jack G. Pennick, Vice President for Business Affairs

Arizona State University
Tempe, Arizona
April 15, 1976

DISCLAIMER

NOTICE

TABLE OF CONTENTS

ADDENDUM TO PROGRESS REPORT

(Included separately)

Reprints + Preprints Removed

Submitted and in Press

1. "The Structural Chemistry of Some Complex Oxides: Ordered and Disordered Extended Defects," LeRoy Eyring and Leung-Tak Tai, in "Treatise on Solid State Chemistry," B. Hannay, Ed., Plenum Publ., COO-1109-76. (Title page and Table of Contents only)

2. "Oxygen Transport in Polycrystals and Single Crystals of Iota Phase Praseodymium Oxide," K. H. Lau, D. L. Fox, S. H. Lin and L. Eyring, High Temp. Chem., COO-1109-79. (Title page and Abstract only)

3. "The Crystal Structure of $Pr(OH)_2NO_3$," M. Lundberg and A. J. Skarnulis, Acta Cryst., COO-1109-85. (Title page and Abstract only)

Reprints

1. "On the Crystal Structure of the Fluorite-Related Intermediate Rare Earth Oxides," P. Kunzmann and L. Eyring, J. Solid State Chem., 14, 229-237 (1975). COO-1109-80.

2. "Chemical Hysteresis in Phase Transitions in the Terbium Oxide-Oxygen System," A. T. Lowe and L. Eyring, J. Solid State Chem., 14, 383-394 (1975). COO-1109-81.

3. "The Effect of Crystal Size on Chemical Hysteresis in Praseodymium and Terbium Oxides," A. T. Lowe, K. H. Lau and L. Eyring, J. Solid State Chem., 15, 9-17 (1975). COO-1109-82.

ABSTRACT

The central theme of this research is to elucidate the structure of real solids. The rare earth oxides are the model systems of choice because they exhibit the full range of structural variability; are representative of the ubiquitous and much studied fluorite structure; and are models for many materials needed for new energy source applications.

It has been demonstrated that electron microscope images obtained at about 3Å resolution for Pr_7O_{12} are in agreement with calculated images based upon known structures. This establishes the efficacy of crystal structure image interpretation in structural terms, including the defect structure and mechanism of phase reactions, for these types of related phases whose structures are as yet beyond conventional means to determine.

Further work on the epsilon ($Pr_{10}O_{18}$) phase is reported both utilizing electron optical methods and single crystal X-ray techniques. The ternary ceramic system $HfO_2 \cdot xEr_2O_3$ is being examined using electron optical techniques and ordering not hitherto reported is being observed.

An interactive crystal structure image calculation system

is being developed which will permit the immediate comparison of enhanced images synthesized from trial structures (including defects) and displayed in juxtaposition on a graphics unit.

CONTRACT REQUIREMENTS

The contract requirements have been fully complied with.

EFFORT OF PRINCIPAL INVESTIGATOR

The principal investigator devoted 20% of his time during the nine-month academic year, September-May, and 80% of two and one-half months, June-August to Project E(11-1)-1109.

I

SUMMARY

In this report an effort has been made to place the work on the solid state chemistry of rare earth oxides, done with the aegis of ERDA, against the primary responsibility of that administration. To this end the first and longest section has been written. This section will be published in the proceedings of the symposium on "Solid State Chemistry of Energy Conversion and Storage" held in conjunction with the Centennial meeting of the American Chemical Society in New York in April 1976.

If reactions in solids are to be understood, the real structures of the reactants and products as well as the nature of the materials in transition must be known. The emphasis is placed upon real solids to stress the importance of cataloging the defect types present at each stage of reaction. A realistic reaction mechanism must be based upon the species known to exist. Taxonomy must preceed the theory of evolution. The purpose of the work being carried out in our laboratory is to answer

these questions for fluorite-related materials by using the rare earth oxides as model systems.

Fluorite-related materials of wide compositional variability are among those most commonly encountered in energy storage and conversion processes. A general characteristic of oxides in this family is that their metal substructure is rigid and immobile while the oxygen substructure is labile and volatile which makes them useful for those applications that require high oxygen diffusion rates or activities but limits the usefulness of many of them where variability of composition is a problem at high temperature.

Zirconia, hafnia, thoria, urania and ceria react with the alkaline earth and rare earth oxides to form solids with compositions over the entire range from MO_2-M_2O_3. Attention is directed in this discussion to intermediate phases which vary smoothly over a composition range such as the $MO_{1.5+\delta}$ and $MO_{2-\delta}$ type phases at high temperature, or order in phases of narrow composition range at low temperature. There are examples of these materials which are of practical importance as solid electrolytes, electrodes, oxygen activity probes and oxygen sources. These are discussed particularly with respect to the existence of ordered intermediate phases. For example, solid solutions of U_3O_8 and Y_2O_3 are excellent electronic conductors under oxidizing or reducing conditions hence are potential electrodes for high-temperature fuel cells. The oxygen conductor $ZrO_2 \cdot xY_2O_3$ which is also fluorite-related could serve as the electrolyte.

The ordered intermediate phases not only have a fluorite-like substructure in common but many of their structures are becoming known and the patterns of defect interactions are beginning to suggest themselves.

The nuclear fuels $UO_{2-\delta}$, $PuO_{2-\delta}$ and $(U, Pu)O_{2-\delta}$ and other actinide oxides also belong to this structural family. Recent studies in these systems are indicating a great deal of short-range order even at high temperature. This order suggests interactions between defect species which no doubt closely resemble those being described in the rare earth oxide systems. This is most marked in the behavior of the heavy members of the actinide series, especially curium and californium.

There is a remarkable behavorial carryover between the many fluorite-related systems whether binary or ternary.

If the importance of the knowledge of the real structure of solids is accepted it would be difficult to overestimate the value to the study of solid state reactions of a technique which would give direct visual representations of not only the structures of the ordered reactants and products but also of the reaction stages in between. The high resolution electron microscope appears to go a long way toward fulfilling this need.

Until the present, in the absence of direct methods, indirect ones have given every conceivable answer to the question of what type of defect species exist. Even if the electron optical methods have their own limitations the information they are bringing to the subject is revolutionizing our views of solid state chemistry. Actually the whole subject of mechanisms of reaction and diffusion will have to be completely revamped in all cases where the defect concentration is greater than a few parts per million.

High resolution electron optical techniques have had astounding success in imaging transition metal oxides having unit cells which are short in the direction of viewing but large in the other two directions. It remained to be determined to what extent the technique could be applied where these favorable circumstances are not met, which is the situation for most materials. The success to date on the rare earth oxides in these laboratories appears to give an affirmative answer and is reviewed in some detail.

A computer program package has been developed which can be used to calculate the two-dimensional crystal structure images necessary to serve as a guide in interpreting the images observed in studies of the rare earth oxide phases and their reaction processes. This is very important since the images obtained for crystals > 100Å thick do not have a one-to-one correlation with the projected potential of the structure. The periodicity and symmetry are retained however, hence the images unmistakably reflect the phases present. The computing package was applied to Pr_7O_{12} and to the isostructural $Zr_3Sc_4O_{12}$ whose structure appears to be the protype for the homologous series (R_nO_{2n-2} where n is an integer) in the binary fluorite systems.

Earlier electron diffraction and imaging studies on the homologous series had revealed the unit cells of most members and had made possible suggesting a structural principle which related the odd members of the series. These studies now have been extended to image, calculate and discuss $Pr_{12}O_{22}$ and other even-members of the series and to propose a structural feature, characteristic of the even-members, which links them to those with odd n.

Although this work is advancing an understanding of the structures of these phases, the ideal structures must be determined by neutron or X-ray diffraction. These techniques are being applied wherever possible. The main limitation at present is the growth of twin free single crystals. It has been possible to prepare good small single crystals of the epsilon phase ($Pr_{10}O_{18}$) and a full set of X-ray diffraction data have been collected and are being analyzed. It is essential to determine the structure of certain key members of the series to provide the basis of generalizing their relationships. As each plausible structure is tested against the diffraction data its structural image is calculated and compared with the observed images. In this way it is hoped that an unequivocal answer will be obtained.

Electron optical techniques have further been applied to the observation of phase reactions occurring in the microscope as one member of the homologous series transforms into another. The main advance so far has been to observe the texture and topotaxy of these reactions and many surprising results have been obtained. For example, among the homologous series cooperative transformations appear to occur along reaction fronts consisting of {135} in odd and {011} in even-members rather than by the traditional nucleation and growth. This results in disordered and especially intergrown materials during reaction. Sometimes layers of phases one unit cell thick are interleaved regularly for a distance then stacking disorder occurs. Gradually the textural characteristics of these reaction intermediates are being cataloged and out of this will come a reliable model for fluorite reaction mechanisms.

To advance the work further it will be necessary to model the structural features at the interface as reaction proceeds. To do this reliably will require companion calculations to be made. This means that one may need to calculate the expected image when one structure is superimposed on another or as defects are moved about during reaction and compare these results with observations. To accomplish this an interactive crystal structure image calculation and observation system is being assembled and placed into use.

The system consists of a Syntex Analytical Instruments AD-1 Autodensitometer operated by a Data General Nova 1200 computer with 24K words of memory and a 9-track tape drive. A Tektronix 4010 graphics unit is interfaced to the Nova computer enabling the crystal structure images observed or calculated to be displayed immediately.

The system will allow an image plate to be scanned, digitized and an enhanced image displayed. The calculated image may then be displayed alongside while the trial structure on which it is based is changed until satisfactory agreement is observed. This rapid interactive scheme is required if the technique is to be a practically useful analysis of this type. At the moment the formidable software development is underway.

The microdensitometer facility will also be used to analyze and compare observed and calculated diffraction patterns where advantageous. In fact, studies underway on ordering in the ternary phase $Er_2O_3 \cdot xHfO_2$ is a case in point. Phases with high HfO_2 content annealed at 1200°C for long periods of time produce extensive weak diffuse scatter in the electron diffraction patterns. The nature of this ordering may be understood by comparing the observed diffraction pattern with that calculated on the basis of various models which, for example, may involve ordered domains of certain structures and sizes intergrown in the fluorite matrix. When the microdensitometer system is completely operable it will be a powerful aid in the analysis of electron optical and X-ray diffraction results.

A recapitulation of conclusions and advances may be made as follows:

1. Crystal structure images of good resolution have

been obtained from crystals of several phases in the homologous series of fluorite-related oxides.

2. The calculated images of thin crystals correspond to the projected potential of the known structure.

3. The observed images correlate well with those calculated for thick crystals where the structure is known.

4. The thick crystal images do not provide an intuitively interpretable picture but the correlation of periodicity and symmetry affords unequivocal identification of the phases observed.

5. Phase reactions can be followed in substantial detail, however more must be done to model them accurately.

6. It will be necessary to continue to use calculated images to minimize errors in interpretation.

7. In systems where thin crystals may be observed intuitive interpretation should be possible even to the point of locating oxygen vacancies in fluorite-related crystals.

8. It has been possible to prepare good single crystals of the rare earth oxides for X-ray study. It is

imperative that both techniques be used in their study to provide enough information.

9. An interactive image reading, image calculating and display system is being developed which will facilitate reliable interpretation of the electron optical results. It will also serve to compare the observed and calculated electron or X-ray diffraction patterns in a similar way.

10. More information about the structures of intermediate phases in fluorite-related materials is becoming available from many sources. At the moment the complexity is baffling but with sufficient effort structural interrelations will be divined and order will replace chaos.

II

NONSTOICHIOMETRY, ORDER AND DISORDER IN FLUORITE-RELATED MATERIALS FOR ENERGY CONVERSION

ABSTRACT

Fluorite-related materials occur widely and many are useful in the new energy source technology. Examples include fast ion conductors such as solid solutions of the alkaline earth or rare earth oxides with zirconia, hafnia, ceria or thoria. Others such as UO_x, PuO_x and $U_xPu_yO_z$ are possible nuclear fuels. Formulating realistic transport and reaction mechanisms in these substances require a knowledge of the defect structure and texture of the ordered and disordered phases. Modern high resolution electron optical methods have been utilized to deduce the unit cells of many ordered intermediate phases in fluorite-related systems and coupled with extant structural information has allowed a structural principle underlying the homologous series in the rare earth binary system to be promulgated. In addition, crystal structure imaging

at a resolution of 3-4Å coupled with comparisons with calculated images have made it possible to propose unknown structures and to observe and model the types of intergrowth patterns and defects which occur. Intermediate and defect structures in fluorite-related oxides of interest here are reviewed. The new results on rare earth oxides are discussed and illustrated including display and modeling of images of crystals unreacted and undergoing transition. The results for the binary oxide studies are compared with the ternary fluorite-related oxides obtained by these and other means.

INTRODUCTION AND REVIEW

The structure of a material is an encyclopedia on the properties of its constituent atoms and is therefore at the root of all its chemical and physical properties. We mean, of course, the structure of the real material which includes its defects most responsible for the reactivity and dynamics of chemical and physical change. Mechanism in reactions cannot be understood without knowledge of the defect structure. Understanding can lead to improved control of reaction properties and to the ability to design new desirable materials.

It is important therefore to elucidate the structure of real materials of practical importance in the most direct way possible and these studies will serve as a basis of further understanding. One seeks here not a shallow classification but deep insight of subtle shading.

Fluorite-related materials are among those commonly encountered in energy conversion and storage. Their varied usefulness and their limitations can best be understood in terms of their structure which is a palpable expression of their nature.

The fluorite structure may be visualized in many ways. For example, if all the tetrahedral interstices in a cubic close-packed array of atoms are filled by atoms of a different kind, the fluorite structure is obtained. The lattice is face-centered cubic (<u>Fm3m</u>) with metal atoms (M) at (0, 0, 0) and the nonmetal atoms (X) at $(\frac{1}{4}, \frac{1}{4}, \frac{1}{4})$ and $(\frac{1}{4}, \frac{3}{4}, \frac{1}{4})$ and equivalent positions. This gives four formula units per unit cell.

An alternative way of visualizing the structure is to consider the coordination cubes of the metal atoms (MX_8) sharing all edges in a three-dimensional chessboard network, or further that coordination tetrahedra of nonmetal atoms (XM_4) share all edges in a nonspace-filling three-dimensional network.

Still another way of expressing this structure is to consider it as a stacking of close-packed layers of atoms along the [111] direction in the sequence α B γ β C $\alpha\gamma$ A β α B γ β C α . . . where Roman capitals represent metal atoms and Greek letters nonmetal, each in equally spaced cubic close-packed layers. Figure 1 illustrates a unit cell of fluorite where circles represent metal atom positions and triangles represent nonmetal atom positions. The octahedral interstices representd by the diamonds are all empty.

Textbook examples of the fluorite structure are usually the fluorides of Ca, Sr and Ba and the oxides of Th and U. To this list must be added many others where the atom radius ratio of metal/nonmetal ≥ 0.73. These would include many of the hydrides and oxides of the rare earth and actinide elements as we shall see later. Furthermore, when we consider adding or subtracting atoms of either type to give fluorite-related defect structures which may be ordered or disordered the possibilities boggle the mind.

Fluorite-related materials have a known compositional variation at least from M_4X_9 ($MX_{2.25}$) to MX. Although there are many other fluorite-related materials of importance in energy conversion, such as the fluorides and hydrides, we here shall be focusing attention almost exclusively to oxygen-deficient phases in the composition range MO_x ($2.0 \geq x \geq 1.5$) where the oxygen deficiency is either ordered or disordered.

In these phases it will be a good approximation to consider the metal atom substructure to be intact as in fluorite with small displacements understood. The oxygen substructure is then characterized as possessing vacancies on normal sites which may be ordered in long or short range or disordered. This means that there will always be coherence but there may be a regular or periodic variation in oxygen composition in the structure.

Many metals capable of tetravalency form extremely thermally stable fluorite-related oxides. Indeed, ThO_2 is the highest melting oxide known (3300 ± 100°C). The congruently melting compositions of all these refractory oxides in vacuum is lower than the dioxide (even for ThO_2). CeO_2 loses oxygen in vacuum to a composition of $CeO_{1.51}$ at 2000°C in a tungsten cell and Pr and TbO_2 lose oxygen to substoichiometric $MO_{1.5-\delta}$ at the melting point. The melting point of reduced substances is in excess of 2000°C.

The enthalpies of formation of the oxides for the elements forming fluorite-related phases is very high being of the order of 210-260 kcal/gram atom of metal.

A few other general statements about properties should be made at this time. Diffusion coefficients of metal atoms are generally very low up to temperatures in excess of one-half the melting point, in contrast the diffusion coefficients of the oxygen atoms are relatively very large. Under these same conditions the vapor in equilibrium with the solid is oxygen. Much higher temperatures must be attained before metal containing vapor species are detectable. In short, the metal substructure is rigid and nonvolatile while the nonmetal substructure is mobile and volatile.

FLUORITE-RELATED MATERIALS* IN ENERGY WINNING ROLES

Solid Electrolytes

Zirconia and Hafnia based materials.--When zirconia or hafnia are reacted with the alkaline earth oxides (especially calcia) or rare earth oxides pseudobinary fluorite-related phases with anion vacancies are formed. At high temperatures the phase fields are broad cubic solid solutions although in some cases there may be considerable diffuse scatter in their diffraction patterns. These materials are technically important because of the rapid transport of oxide ions at moderately high temperatures without electronic or cation conduction. This assures a wide variety of high temperature electrochemical uses.

At higher temperatures cubic phases of continuously changing composition cover the field. At lower temperatures, $\leq$ 1500°C, in a few cases known so far ordering occurs, probably rapidly with respect to the anion vacancies and with sufficiently long anneals, the cations may also order.

---

*There is a romantic history and great literature on these anion deficient fluorite-related phases. This includes Welsbach gas mantles and Nernst glowers. This paper is not intended to be comprehensive; rather references are made arbitrarily to that work which highlights current efforts to clarify the structural principles behind defect fluorite-related materials.

Duclot, Vicat and Deporter[1] tabulate the investigations of calcia and rare earth fluorite-related phases formed separately with hafnia and zirconia up to about 1970. They also give evidence of an ordered phase $Y_2Hf_7O_{17}$ and have investigated the order-disorder transition.

Carter and Roth[2] have studied the structure of calcia-stabilized zirconia utilizing neutron diffraction. They concluded that in the ordered structure the oxygen atoms were displaced in a way approaching that found in monoclinic ZrO_2. The disorder-order transition was seen to be the differentiation of the disordered region into domains in which the distortions of the oxygen coordination polyhedron are in the same sense.

Three ordered phases (Φ, Φ_1, Φ_2) were detected in the CaO-HfO_2 system,[3] two of which (Φ_1 and Φ_2) appear also in CaO-ZrO_2.[4]

Allpress, Rossell and Scott have investigated the ordered phases[5] in the calcia-stabilized hafnia system using electron diffraction to determine the unit cells of three ordered phases: $Ca_2Hf_7O_{16}$ (Φ), rhombohedral, $\underline{a} = 9.5273$Å, $\alpha = 38.801°$; $CaHf_4O_9$ (Φ_1), monoclinic, $\underline{a} = 17.698$Å, $\underline{b} = 14.500$Å, $\underline{c} = 12.021$Å and $\beta = 119.47°$; and $Ca_6Hf_{19}O_{44}$ (Φ_2), rhombohedral, $\underline{a} = 12.059$Å, $\alpha = 98.31°$. Rossell and Scott[6] determined the space group of Φ phase to be $\underline{R\bar{3}}$ and have found cations ordered on cation sites of the fluorite structure with the calcium ions segregated into discrete layers parallel to the (111) fluorite plane. They also suggest that the two oxygen vacancies in the unit cell are paired across the body diagonal of the coordination cube of one of the Hf atoms and the remaining six Hf atoms are near neighbors and seven-coordinated while the calcium atoms are eight-coordinated.

Subsequently Allpress, Rossell and Scott[7] have published the structure of $CaHf_4O_9$ (Φ_1) and $Ca_6Hf_{19}O_{44}$ (Φ_2). As in the Φ phase the Ca atoms are all eight-coordinated while Hf may be six-seven- or eight-coordinated. Other common features include probable $\frac{1}{2}\langle 111\rangle_F$ vacancy pairs with a cation in between. Allpress, et al., suggest that these clusters may coalesce to form finite groups in Φ_1 or extended chains in Φ_2. This information was obtained from powder diffraction data which affords only limited conclusions about vacancy ordering.

Electron diffraction patterns of calcia stabilized hafnia and zirconia show diffuse scatter in addition to the strong reflections from the fluorite subcell. Allpress and Rossell[8] have analyzed this diffuse scatter and obtain good agreement with the expected diffraction from specimens with domains of the Φ_1 phase of 30Å diameter coherently embedded in specific orientations within the cubic matrix. This is reminescent of the domains of Carter and Roth.[2]

Lefevre[9] noted ordering in ZrO_2-Sc_2O_3 due to a phase which turned out to be rhombohedral $Zr_3Sc_4O_{12}$[10] and two others with wider composition widths and higher ZrO_2 content. Bevan[11] and his coworkers have determined that the composition width of these phases is less than at first thought and have assigned them the ideal formulas $Zr_3Sc_4O_{12}$, $Zr_{10}Sc_4O_{26}$ and $Zr_{48}Sc_{14}O_{117}$. $Zr_3Sc_4O_{12}$ was found[12] to be isomorphous with M_7O_{12} in the binary phases to be described later. The structural feature emphasized in these results is a string of oxygen vacancies along the $[111]_F$ which gives units of M_7O_{12} composed of a six-coordinated M atom surrounded with trigonal symmetry by six seven-coordinated M atoms. These units are separated by a fully oxidized M_7O_{14} group along $[111]_F$-like beads of two types in a string to form the structure of $Zr_{10}Sc_4O_{26}$ (space group $\underline{R\bar{3}}$). These beaded strings all oriented parallel to the threefold axis are edge shared to form an interpenetrating network of the two kinds of units. The Zr and Sc atoms occupy the metal sites randomly in both structures.

In the $Zr_3Yb_4O_{12}$ phase,[13] where the larger Yb is present, two modifications are observed. One is isostructural with $Zr_3Sc_4O_{12}$ and the other (a low temperature form) has some ordering of metal atoms with Zr occupying the six-coordinated metal sites and random occupancy of the seven-coordinated sites. In the other rare earth zirconia solid solutions [11] where the size discrepancy between the atoms increases there appears to be little evidence of ordering.

It is likely that the ordered phases of similar composition observed by Komessarova and Spiridinov[14] in the HfO_2-Sc_2O_3 system and indexed as rhombohedral unit cells are closely related to these $ZrO_2 \cdot Sc_2O_3$ phases.

Collongues and coworkers[10, 15] and many others[1] have found pyrochlore phases in these ternary oxide systems. Although this phase, $A^{3+}_2B^{4+}_2O_7$, is related to fluorite, the shifts in oxygen positions are so great that the structure is best considered as interpenetrating frameworks of $[AO_2]$ and $[BO_6]$ with the A in linear coordination and B in octahedral coordination. The radius ratio, $r(A^{3+})/r(B^{4+})$, is between about 1.20 and 1.60.

<u>The Thoria-Rare Earth Oxide Systems</u>.--Solid solutions between thoria and the rare earth oxides are well known and have been used for years as oxygen conducting solid electrolytes. In each case studied there is a wide range solid solution having a fluorite structure up to a maximum at moderate temperatures

of about 40% (M_2O_3) in ThO_2. No ordered intermediate phases in this system at low temperatures have been described.

On the M_2O_3-rich side at very high temperatures however Sibieude and Foex[16] have found evidence of a quite remarkable complexity showing phases related to the A, B, C, X and H-type sesquioxides of variable composition as well as numerous other hexagonal phases of apparent narrow composition. The C-type phase is, of course, fluorite related but no ordered intermediate narrow composition phases have so far been indicated in the ternary system.

<u>The Uranium Dioxide-Rare Earth Oxide Systems.</u> --Weitzel and Keller[17] have recently prepared several oxides of composition $(M_{0.5}U_{0.5})O_2$ where M is a rare earth atom, and have shown them to be strictly fluorite in spite of the unusual presence of U(V) and U(VI) in eight-coordination.

Many studies have shown the formation of fluorite solid solutions of wide composition range. Our attention is drawn to $3Y_2O_3 \cdot UO_3$ or UY_6O_{12} which was the first crystal of this structure determined.[18] It is isostructural with the $Zr_3M_4O_{12}$ phases discussed above and with the binary oxides of composition M_7O_{12} to be discussed below as the structural end member of the homologous series in the rare earth higher oxides. So far as is known these are the only ordered fluorite-related ternary oxides in this family.

Fluorite-Related Oxides for the Nuclear Industry

Many reactor fuels and radiation power sources are fluorite-related oxides. These substances characteristically must operate in place for long periods of time, at high temperatures, in strong radiation fields and with growing levels of impurity. Underlying any rationally based program to improve the performance characteristics of these materials must be a sound knowledge of their structure and texture, especially their defect structure, as a function of temperature, pressure of oxygen, radiation field and level of impurity.

Attention will be focused here on the structures of oxygen-deficient fluorite-related oxides of the actinide elements. This includes UO_2, ThO_2, PuO_2 $(U, Pu)O_2$ as well as the trans-uranium oxides.

Fluorite $MO_{2-\delta}$. --Dioxides are known for Th, Pa, U, Np, Pu, Am, Cm, Bk and Cf. The lattice parameters are compared in Figure 2. The enormous variation of the thermodynamic stability is reflected in the oxygen activity required to maintain stoichiometry at 1000°C which varies more than 20 orders of magnitude.

ThO_2 is only slightly substoichiometric in the presence of Th even near the melting point. UO_2 begins to lose oxygen appreciably in the presence of U at about 1500°C and reaches a eutectoid at 2500°C at a composition of about $UO_{1.65}$. The heavier actinide dioxides typically show little deviation from stoichiometry until a temperature of a few hundred degrees is reached and then quite suddenly a phase of wide composition range of fluorite structure is entered. The degree and nature of short or long range ordering of defects in these $MO_{2-\delta}$ phases have not progressed very far. A brief review of work up to about 1970 along these lines offers phase diagrams and references.[19]

Recently Sørensen[20] has undertaken measurements (and the correlation of the work of others) of the partial molar thermodynamic quantities for oxygen in nonstoichiometric plutonium and plutonium-uranium oxides. He has previously done a similar analysis on the $CeO_{2-\delta}$ system.[21] In each of these systems a careful analysis of the thermodynamic data shows surprising deviations from ideal solution. In each case a derived phase diagram indicates several subregions in the $MO_{2-\delta}$ phase in which the slopes of $\Delta\overline{G}_{O_2}$ vs log X have characteristic values. In the $CeO_{2-\delta}$ phase in addition to numerous nonstoichiometric subregions within which consistent thermodynamic properties are observed, there are superimposed indications of stability at particular stoichiometries belonging to a homologous series M_nO_{2n-2}. In the PuO_x system three such subregions (from PuO_2-$PuO_{1.82}$) and two two-phase regions are indicated. The two-phase regions are in the composition range $PuO_{1.9945}$ and $PuO_{1.9998}$. The $(U, Pu)O_{2-\delta}$ phase separates, by the same treatment, into five subregions with no indication of special stability at any narrow composition. The results cover the composition range $2.00 > x > 1.85$.

High temperature X-ray diffraction observation[20, 21] in these systems have shown superstructures of monoclinic symmetry about 900°C in the CeO_{2-x} system. However, in $PuO_{2-\delta}$ or with an admixture of urania only fluorite structures were formed. It seems apparent that even at these high temperatures (although only up to little more than one-half the melting temperatures) that there is considerable order, at least short-range order. This order exists in spite of a high mobility of oxygen atoms which at the highest temperatures must spend a good deal of time between positions of minimum energy.[22]

The M_7O_{12} phase has definitely been established for Cm and Cf[23, 24] and there is clear evidence for order in intermediate regions in the $CmO_{1.82}$ and at two compositions in the $BkO_{2-\delta}$ system.[25]

Table I summarizes the known intermediate phases among the actinide oxides in MO_x $1.5 < x < 2.0$. The names of the phases are used advisedly following the nomenclature for the lanthanide oxides.

In summary it is clear that many of the fluorite-related actinide oxides exhibit wide range nonstoichiometry at high temperatures with an apparent tendency to at least short-range order which at low temperatures in the heavier members gives ordered intermediate phases of narrow composition range. Evidence for ordering in these materials is growing steadily.

A word should be said about the σ phase ($MO_{1.5+\delta}$) which is observed in several of the actinide oxide systems as well as in the rare earth-zirconia, hafnia or thoria systems. This is a phase of variable composition related to the C-type rare earth sesquioxides and is also a prominent feature of the Ce, Pr and Tb oxide systems. In all cases where this phase exists it appears to be separated at high temperatures from the α ($MO_{2-\delta}$) phase by a narrow miscibility gap. Since the metal positions in both phases are essentially those of the fluorite structure it is apparent that in the range of 1200°C the ordering of oxygen determines phase stability.

Fluorite-Related Ordered Phases in the M_2O_3-WO_3 System

Oxides of this type are being considered as phosphors, laser hosts and nuclear control materials. McCarthy, et al.,[26] have reviewed the literature on the crystal chemistry of fluorite-related rare earth-tungsten-oxides. They have prepared fluorite-related compounds of the composition M_6WO_{12}, $M_{10}W_2O_{21}$, $M_{14}W_4O_{33}$. M_6WO_{12} is isomorphous with Y_6UO_{12} but although the other two are thought to be similar to other members of the rare earth series their structures have not been determined.

Structural Characteristics of the CeO_x System

As to be expected the well established higher oxides of cerium possess fluorite-related structures. Many powder diffraction studies of the intermediate phases have been carried out both by quenching the specimens and by high temperature techniques. Table II presents what appears to be the best parameters presently available for the known phases.

Sørensen[21] has reported finding a phase (Ce_6O_{11}) at 900°C isostructural with Pr_6O_{11} with a monoclinic unit cell with $\underline{a} = 6.781 \pm 0.006$Å, $\underline{b} = 11.893 \pm 0.009$Å, $\underline{c} = 15.823 \pm 0.015$Å and $\beta = 125.04 \pm 0.04°$. There has been no verification of the composition however, and the relative intensity of the subcell and supercell reflections do not appear reasonable.

Ray and Cox[27] have recently determined the structure of Ce_7O_{12} by neutron diffraction measurements from powders and single crystals. They confirm the compound to be isostructural with Pr_7O_{12}. The space group is $\underline{R\bar{3}}$ with hexagonal unit cell dimensions $\underline{a}$ = 10.37Å and $\underline{c}$ = 9.67Å (rhombohedral cell $\underline{a}$ = 10.37Å and α = 99.4°). The hexagonal cell contains three formula units of Ce_7O_{12}. An important observation in this study was that the crystals were extensively twinned and these twin domains had to be sorted out. There was a different amount of disorder in powder and single crystal, being greater in the powder. Considerable disorder has been seen in electron micrographs of Pr_7O_{12} hence it may be characteristic of these materials.

Neutron and X-ray powder diffraction patterns of specimens of composition $CeO_{1.710}$, $CeO_{1.781}$, $CeO_{1.822}$ and CeO_2 have been studied by Ray, Nowick and Cox.[28] They confirm distinct structures for these phases establishing $Ce_{10}O_{18}$ (n = 10) for the first time. The structures of phase n = 9 and 10 appear to be different from the unit cells obtained by Kunzmann and Eyring[29] in the PrO_x system. The X-ray results of Height and Bevan[30] give unit cells which are also different from those of PrO_x but it is not known whether they agree with Ray and Cox.[27]

The M_7O_{12} phase is isomorphous in Ce, Pr and Tb oxides and appears to be the lower structural end-member of the M_nO_{2n-2} series. The relationships between the structures of the other members which belong compositionally to the series is not known. It is clear that there are a great number of possible ways of accommodating a deficiency of 1/9, 1/10 or 1/11 of the oxygen atoms.

<u>Structure and Texture in the Binary Rare Earth Oxides</u>

<u>Homologous Series</u>.--Structurally the binary rare earth oxides display a full range of behavior. They exhibit an homologous series of intermediate phases with the generic formula M_nO_{2n-2} where n is an integer between 4 and ∞. (These phases have a small but definite range of composition.) The ordered phases disorder at higher temperatures and oxygen pressures to form compounds of wide composition range which are among the last embattled remnants of grossly nonstoichiometric phases. In addition they also indicate the formation of what have been called pseudophases--regions of two-phase areas where the material behaves monophasicly. Chemical hysteresis is also an almost universal structurally induced characteristic of phase transitions.

High oxygen mobility in these phases together with modest electronic conductivity obviates the need for cation mobility and allows the formation of each phase with astonishing rapidity even at moderate temperatures (> 300°C).

The unit cells for several members of the homologous series M_nO_{2n-2} where n = 7, 9, 10, 11 and 12 have been determined[29] using electron diffraction and added to those already known for n = 4 and ∞. These are shown in projection along $[21\bar{1}]$ in Figure 3 and are described in detail in Table III. In addition polymorphism occurs in the zeta (n = 9) phase and perhaps in others.

All the phases have the same a axis. The arrangement of vacancies along this axis, which is a vector of the kind $\frac{1}{2}[21\bar{1}]_F$, are shown in Figure 4. This feature of the iota structure is considered to be the largest held in common by the members of the homologous series of binary oxides (n = 7, 9, 10, 11, 12). The odd members of the series also have the same c axis hence have the iota ac plane, $(135)_F$, as a common feature. As Figure 3 shows, the even members have an ac plane in common also but c is different in this case. Another element which went into this structural principle hypothesis was the high resolution structure images of the delta phase ($Tb_{11}O_{20}$) which appeared to show (Figure 5) the positions of the vacancies in the unit cell as would be predicted (Figure 6).

In spite of this apparent success application of high resolution crystal structure imaging to structures such as the fluorite type has not previously been developed hence great care must be taken in the interpretation of the images obtained.

High resolution crystal structure imaging has been shown capable of giving a two-dimensional point-to-point image of the crystal potential to a resolution of about 3.5Å. This is possible for crystals when there is a short axis of only one-coordination polyhedron in the direction of viewing and rather large axes in the other two directions. Such a structure exhibits large variations in potential when viewed down this short axis. In addition the crystal must be thin (< 100Å), oriented within about a tenth of a degree, and be viewed at the correct defocus. Under these conditions it has been possible to produce crystal structure images of structures based on the ReO_3 structure for example, capable of intuitive interpretation.[31]

The fluorite superstructures, on the other hand are not likely to exhibit large potential variations in any direction. An added disadvantage is that the shortest axis for these materials is the 6.75Å a axis. This strains the thin phase object approximation on which the calculations are based and hence requires that the technique be shown to apply. To add to the difficulty the reciprocal lattice axes perpendicular to the projection axis are rather long producing few beams in a reasonable sized aperture.

The stakes in success are high, however, since this technique alone can reveal textural details directly and it is vital to be able to treat any important class of substances such as the fluorite materials. It is imperative in view of such unfavorable circumstances to compare calculated and observed images to avoid serious errors in the interpretation.

With this in mind Skarnulis, Summerville and Eyring[32] have tested the applicability of the method on the prototype of the homologous series, the iota phase (Pr_7O_{12}), the only one of the intermediate phases for which complete structural data are available.[33] The n-beam multislice method of Cowley and Moodie[34] is the basis of the image contrast calculations.

CALCULATED IMAGES OF THE IOTA PHASE

(Pr_7O_{12}), $[21\bar{1}]_F$ Zone

Figure 7 shows the projection of the ideal atoms for Pr_7O_{12} when viewed down the $\langle 111 \rangle_F$ and the $\langle 21\bar{1} \rangle_F$ axes. The MO_8

coordination cube is also shown to facilitate orientation.

Calculated n-beam images of the $[21\bar{1}]$ zone for 25, 165 and 235Å thick crystals are shown in Figure 8 using ionic scattering factors. The defect of focus of the microscope is taken to be -1000Å. The origin is placed at the top left-hand corner with two of the axes ($\underline{a} \equiv \underline{b} \equiv \underline{c}$) along the figure edges.

The calculated thin crystal images at 1000Å underfocus correspond to the projection of the columns of oxygen vacancies in the structure--there being two per unit cell in this case. There are a wide variety of images calculated when many thicknesses and defects of focus are used[32] but there is a tendency for thicker crystals to show only one white spot per unit cell (e.g., at 235Å thickness, 1000Å underfocus with ionic scattering factors). This feature correlates with the strings of six-coordinated metal atoms.

It is clear that the images for thicker crystals do not have a one-to-one correlation with the projected potential hence cannot be considered as true crystal structure images. They do however have the periodicity and symmetry of the structure and for this reason are powerful tools in identifying and correlating observed images.

<u>$Zr_3Sc_4O_{12}$, $[21\bar{1}]_F$ Zone</u>

This phase is isostructural with Pr_7O_{12} and for this reason differences in the images may be used to infer differences in form factors of the metal atoms. The n-beam calculations for this phase using atomic scattering factors are shown in Figure 8. Some generalizations can be made. As in the case for Pr_7O_{12} the thin crystal images correlated well with the projected potential (e.g., 24-48Å thickness, 900-1000Å underfocus, atomic scattering factors).[32] The same is true except for a shift in origin for crystals about 165Å thick as observed for Pr_7O_{12}. The images derived using ionic scattering factors are much fringier but images showing two spots per unit cell occur at 120-144Å and 1000Å underfocus.[32] In both cases the thickest crystals show one spot per unit cell.

Calculated Images of Pr_7O_{12}, $[111]_F$ Zone

These images showing an hexagonal array of spots at all thicknesses and defects of focus almost uniformally indicate one spot per unit cell although there is an origin shift in some cases.

THE OBSERVED IMAGES OF THE IOTA PHASE

Images of R_7O_{12} Phases, $[21\bar{1}]$ zone

Figure 9(a) and (b) show typical images of Pr_7O_{12} with one spot per unit cell. Such images are comparable to some of those calculated for thick crystals. Figure 9(c) shows an image of

$Zr_3Sc_4O_{12}$ in which two spots per unit cell appear in the upper right side. This could be a reasonably thin crystal, say 120-144Å to correlate with the calculated images. In general the observed images of the iota phase show variations as do the calculated images but the correlations are not always unambiguous.

Images of Pr_7O_{12} Phases, ⟨111⟩ Zone

There is quite good agreement between calculated and observed images in this zone; Figure 10(a) shows the observed image. The spots can be correlated with columns of six-coordinated cations in the direction of the beam. In Figure 10(b) one may observe two regions of $Zr_3Sc_4O_{12}$ in twin orientation with an overlay of M_2O_3 (C-type) at the twin boundary. The $[111]_F$ zone axis is common to all three regions.

Discussion of the Iota Phase Images

In spite of its limitations this technique shows great promise as a means of correlating calculated and observed images even if the point-to-point correspondence with the projected potential does not exist for the thick crystals imaged so far. It is difficult in these oxygen labile materials to observe thin crystals without composition change in the vacuum of the microscope under the heating of the electron beam. At the least an unambiguous identification can be made of each phase and the image while not intuitively interpretable may give some help in sorting out the structure since images calculated from wrong structures do not agree well. In the case of passive crystals, thin enough samples could be used to observe images with contrast agreeing with the projected potential.

IMAGES OF BETA, EPSILON AND ZETA PHASES

The Observations

Summerville and Eyring[35] have continued high resolution crystal structure imaging of other ordered intermediate phases in an attempt to clarify the structural principle which would elucidate the homologous series in these fluorite-related materials.

The existence of a bifurcated, even-odd, homologous series in the rare earth oxides was clearly indicated in earlier work.[29] It was important to image members of the even group. Some images of the beta phase ($Pr_{24}O_{44}$) are shown in Figure 11. The strong spots at the corners of a rectangle (nearly a square) correspond to one unit cell in this $[21\bar{1}]$ projection (Figure 3). It is clear that there is considerable contrast within the unit cell.

It was apparent that if the triclinic unit cell with n = 12 shown in projection in Figure 3 were twinned along $(110)_F$ the unit cell actually observed would result. Such a unit cell with expected vacancies is shown in Figure 12 in projection.

Images calculated on the basis of this structure, except that the metal atoms about the vacancies were allowed to relax just as they do in iota phase,[32] are shown in Figure 13 for three thicknesses and -900Å defect of focus. The oxygen atoms are not shifted in this calculation except to remove those corresponding to the vacancies.

The calculated images for thin crystals at -900Å defocus correspond to the projected anion vacancies of the model as they did in the case of iota phase, however, images for thicker crystals are quite different. The observed images of Figure 11 correlate quite well with those calculated at a defocus of -900Å and at 162 and 243Å thickness respectively as shown. All things considered the agreement is better than should be expected. At least the P1 structure of Figure 12 is compatible with the observations.

The thermal decomposition temperature of members of the homologous series decreases from iota to beta which is the last of the series observed in PrO_x except for PrO_2. This decrease of thermal stability suggests the possibility of disorder in these phases. Figures 14 and 15 illustrate such disorder. In one case there is a shift in the intensity of certain spots along a definite boundary and in the other there is a loss of the regular repeat pattern over one unit cell.

An image of the epsilon phase ($Pr_{10}O_{18}$) is shown in Figure 17. The corners of the unit cell are sharp spots with considerable detail in the contrast within the unit cell. Images for this phase are presently being calculated but the results are not far enough along to merit discussion.

Figure 17 depicts images of zeta phase. At the top of the Figure a projection of the bc plane is observed to be fairly regularly spaced but with obvious flucuation of the intersites. An intergrowth of iota and zeta with a repeat distance of $\underline{b}_7 + \underline{b}_9$ is clearly discerned at the bottom but in this case with the ab plane projected. The zeta unit cells have two spots per unit cell whereas they are not so distinct in iota. Calculations have not been made for zeta but since two spots per unit cell are seen in the images of delta phase (Figure 5) it may not be surprising to see them in zeta.

Discussion of the Observed Results

The interpretations as set forward here[32] extend the structural model of Kunzmann and Eyring[29] and are consistent with the view that in the odd members of the series every nth $(\bar{1}35)_F$ plane of cations are all six-coordinated with those in between being all seven- or eight-coordinated. The oxygen vacancies on each six-coordinated cation occur along the body diagonal [111] of the coordination cube at an angle of 73° to the $(\bar{1}35)_F$ plane.

In the even members twinning at the unit cell level along $(110)_F$ produces puckered $\{135\}_F$ planes such that their average direction is parallel to $(110)_F$. In the case of beta, for example, there are alternate segments of $(135)_F$ and $(53\bar{1})_F$ planes of six-coordinated cations which make up the b-face of the monoclinic unit cell. These are $(101)_F$ on average.

IMAGES OF PHASE TRANSFORMATIONS AND INTERGROWTH IN FLUORITE-RELATED BINARY OXIDE SYSTEMS

When the rare earth oxides which have appreciable oxygen dissociation pressures at moderate temperatures are studied in the vacuum of the microscope under the heating of the electron beam, phase reactions are not only possible they are inevitable. Therefore during the course of observing images of the ordered phases specimens in the act of transformation were recorded. Summerville and Eyring[32] have observed numerous cases, a few of which will be rehearsed here.

Diffraction Patterns

Streaking along b* is always observed in the diffraction pattern when disorder is observed in the image. Before the streaking becomes extensive it is replaced by the diffraction spots of the new phase. It is very common to find diffraction patterns containing diffraction spots from two or more phases in the same zone indicating the topotactic intergrowth of these phases. These observations suggest that during reaction there is disorder along b which soon is replaced with order in this direction but by more than one phase. Then finally the new phase occurs alone. These changes in the homologous series seem to occur with an advancing front parallel to $\{135\}_F$ or to the puckered planes if the reaction occurs between even members.

Images of Systems in Phase Reactions

Domains of the conventional sort are rarely seen in images of these materials. As mentioned above and as shown in Figure 18(a), among the homologous series a planer reaction front seems most typical. In this case zeta phase is decomposing to iota and alternating layers one unit cell wide suggest the mechanism of reaction. on the other hand, in the Pr_7O_{12}-Pr_2O_3 phase region where the structures are not so closely related coherent intergrowth appears to result from nucleation and growth in a more conventional way as illustrated in Figure 18(b) and Figure 19. The latter is of a $Zr_xSc_yO_z$ composition of about $MO_{1.64}$. The edge of the conventional domains are seen to be quite clean with little disturbance in the semicoherent interface. In Figure 19 perfect register between the

[111] direction of both phases is observed between the $Zr_3Sc_4O_{12}$ substrate and the Sc_2O_3 inclusions of 70Å in diameter.

Disorder in Images

The occurrence of fine scale disorder in images is very commonly observed. At equilibrium the Zr^{4+} and Sc^{3+} in $Zr_3Sc_4O_{12}$ are random and the oxygen lattice regular. Figure 20 shows disorder which may arise from incomplete randomization of the Zr^{4+} and Sc^{3+} in the $Zr_3Sc_4O_{12}$ specimen which leads to disorder in the oxygen substructure. In other cases disorder is apparent on a larger scale giving almost a superstructure repeat pattern. Figure 21 not only shows this kind of disorder in the Pr_7O_{12} matrix but it also shows epsilon and beta (and perhaps Φ') in a crystal of iota. The periodicity characteristics of the ordered inclusions change with time. Figure 22 shows the relative orientation of the intergrown regions in the specimen of Figure 21.

COMMENTS ON THE RESULTS OF STRUCTURE IMAGING OF FLUORITE-RELATED RARE EARTH OXIDES

1. Crystal structure images of good resolution have been obtained from crystals of several phases in the homologous series of fluorite-related oxides.
2. The calculated images of thin crystals correspond to

the projected potential of the known structure.

3. The observed images correlate well with those calculated for thick crystals where the structure is known.

4. The thick crystal images do not provide an intuitively interpretable picture but the correlation of periodicity and symmetry affords unequivocal identification of the phases observed.

5. Phase reactions can be followed in substantial detail however more must be done to model them accurately.

6. It will be necessary to continue to use calculated images to minimize errors in interpretation.

7. In systems where thin crystals may be observed intuitive interpretation should be possible even to the point of locating oxygen vacancies in fluorite-related crystals.

GENERAL COMMENTS

Fluorite-related materials are important to new energy conversion and storage procedures. Some of these are binary, others ternary or even more complex. They involve many metal atoms and usually oxygen, fluorine or hydrogen. Significant improvement in existing materials and the creation of new materials are required as fossil fuels which have been the conventional sources of energy are displaced.

Central to this materials evolution is a knowledge of structural details at the unit cell level. Such information is needed to understand their function and failure and to direct the process of generating alternatives.

Although the fluorite structure itself is ubiquitous and simple almost all materials of use having structures related to it have extended defects. A review of these ordered and disordered phases has been sketched. It has revealed a multitude of phases of fine scale compositional variability with undoubted short-range order and in addition a multitude of ordered intermediate phases which are often compositionally members of an homologous series M_nO_{2n-2}.

Many details of this homologous series in the rare earth oxide system have been discussed--principally those aspects which have been discovered by means of high resolution electron optical techniques. This has included the determination of the unit cells of the homologues. The use of calculations to give confidence to image interpretation has been demonstrated. The images then can be used to show reaction patterns and disorder in phase reactions.

Finally, recent results on the Ce_nO_{2n-2} series was presented to illustrate that even in this closely related oxide system not all the homologues have the same structure as those of PrO_x or TbO_x.

It appears that much remains to be done before a clear understanding of the manifold of structures which are called fluorite-related is evoked but the quest will be worth the effort.

ACKNOWLEDGEMENT: The current support of the United States Energy, Research and Development Administration (and earlier support of the United States Atomic Energy Commission) for that part of the work described here attributed to the author and his coworkers is gratefully acknowledged.

REFERENCES

1. M. Duclot, J. Vicat and C. Deporter, J. Solid State Chem., 2, 236 (1970).

2. R. E. Carter and W. L. Roth, in "Electrochemical Force Measurements in High Temperature Systems," (C. B. Alcock, Ed.) pp. 125-144, Institution of Mining and Metallurgy, London (1968).

3. C. Delamarre, Rev. Int. Hautes Tempes et Refract., 9, 209 (1972).

4. D. Michel, Mat. Res. Bull., 8, 943 (1972).

5. J. G. Allpress, H. J. Rossell and H. G. Scott, Mat. Res. Bull., 9, 455 (1974).

6. H. J. Rossell and H. G. Scott, J. Solid State Chem., 13, 345 (1975).

7. J. G. Allpress, H. J. Rossell and H. G. Scott, J. Solid State Chem., 14, 264 (1975).

8. J. G. Allpress and H. J. Rossell, J. Solid State Chem., 15, 68 (1975).

9. J. Lefevre, Ann. Chem., 8, 135 (1963).

10. R. Collongues, F. Queipoux, M. Perez y Jorba and J. C. Gilles, Bull. Soc. Chem. France, 1141 (1965).

11. M. R. Thornber, D. J. M. Bevan and E. Summerville, J. Solid State Chem., 1, 545 (1970).

12. M. R. Thornber, D. J. M. Bevan and J. Graham, Acta Cryst., B24, 1183 (1968).

13. M. R. Thornber and D. J. M. Bevan, J. Solid State Chem., 1, 536 (1970).

14. L. N. Komissarova and F. M. Spiridinov, Dokl. Akad. Nauk, SSSR, 182, 834 (1968).

15. R. Collongues, M. Perez y Yorba and J. Lefevre, Bull. Soc. Chim. France, 70 (1961).

16. F. Sibieude and M. Foex, J. Nucl. Mat., 56, 229 (1975).

17. H. Weitzel and C. Keller, J. Solid State Chem., 13, 136 (1975).

18. S. F. Bartram, Inorg. Chem., 5, 749 (1965).

19. L. Eyring, in "Solid State Chemistry (C.N.R. Rao, Ed.) Marcel Dekker, Inc., New York (1974) pp. 565-634.

20. O. T. Sørensen, paper presented at the "Fifth International Conf on Plutonium and Other Actinides," Sept. 1975, in Baden-Baden, Germany. To be printed in Conf. Proc.

21. O. T. Sørensen, J. Solid State Chem., in press.

22. M. O'Keeffe, in "Fast Ion Transport," (W. van Gool, Ed.) North Holland (1973) pp. 233-247.

23. T. D. Chikalla and R. P. Turcotte, NBS Special Pub., 364, 319 (1972).

24. R. P. Turcotte and R. G. Haire, Private communication.

25. R. P. Turcotte, T. D. Chikalla and L. Eyring, J. Inorg. Nucl. Chem., 33, 3749 (1971).

26. G. J. McCarthy, R. D. Fischer, G. G. Johnson, Jr., and C. E. Gooden, in NBS Spec. Pub. 364, 397 (1972).

27. S. P. Ray and D. E. Cox, J. Solid State Chem., 15, 333 (1975).

28. S. P. Ray, A. S. Nowick and D. E. Cox, J. Solid State Chem., 15, 344 (1975).

29. P. Kunzmann and L. Eyring, J. Solid State Chem., 14,

229 (1975).

30. T. M. Height and D. J. M. Bevan, Private communication.

31. S. Iijima, Acta Cryst., A29, 18 (1973).

32. A. J. Skarnulis, E. Summerville and L. Eyring, to be published.

33. R. B. Von Dreele, L. Eyring, A. L. Bowman and J. L. Yarnell, Acta Cryst., B31, 971 (1975).

34. J. M. Cowley and A. F. Moodie, Acta Cryst., 10, 609 (1957).

35. E. Summerville and L. Eyring, to be published.

TABLE I

Intermediate Phases among the Actinide Oxides

M	$MO_{1.5+\delta}(\sigma)$	$MO_{1.71}(\iota)$	$MO_{1.82\pm\delta}(\delta)$	$MO_{2.0-\delta}(\alpha)$
Th				X
Pa				
U				X
Np				X
Pu	X			X
Am	X			X
Cm	X	X	X	X
Bk	X	← indications of order	→	X
Cf	X	X		X

TABLE II

Cell Parameter Data for the Ce_nO_{2n-2} Series[30]

Phase	Unit Cell	Fluorite-Type Psuedocell
Ce_2O_3 (θ)	Hexagonal $\underline{a}_o$ = 3.8905 ± 0.0003Å $\underline{c}_o$ = 6.0589 ± 0.0003Å	No pseudocell
Ce_7O_{12} (ι)	Rhombohedral $\underline{a}_r$ = 6.784Å α_r = 99.302° Hexagonal representation $\underline{a}_h$ = 10.3410 ± 0.0007Å $\underline{c}_h$ = 9.6662 ± 0.0006Å	Rhombohedral $\underline{a}_F$ = 5.5443 ± 0.0004Å α_F = 89.642 ± 0.000°
Ce_9O_{16} (ζ)		Triclinic $\underline{a}_F$ = 5.5106 ± 0.0012Å $\underline{b}_F$ = 5.5155 ± 0.0012Å $\underline{c}_F$ = 5.5213 ± 0.0012Å α_F = 90.339 ± 0.000° β_F = 90.595 ± 0.000° γ_F = 90.204 ± 0.000°
$Ce_{10}O_{18}$ (ϵ)		Triclinic $\underline{a}_F$ = 5.5076 ± 0.0009Å $\underline{b}_F$ = 5.5100 ± 0.0009Å $\underline{c}_F$ = 5.5112 ± 0.0008Å α_F = 90.360 ± 0.000° β_F = 90.176 ± 0.000° γ_F = 90.160 ± 0.000°
$Ce_{11}O_{18}$ (δ)		Rhombohedral $\underline{a}_F$ = 5.5023 ± 0.0007Å α_F = 89.762 ± 0.000°
CeO_2 (α)	Face Centered Cubic $\underline{a}_o$ = 5.4109 ± 0.0003Å	Cubic $\underline{a}_F$ = 5.4109 ± 0.0003Å

TABLE III

Strucmediate Rare Earth Oxide Phases

Composition	n (in R_nO_{2n-2})[a]	Symmetry	Lattice parameters	Relation to basic structure	Relative volume	No. of vacancies/ unit cell
$RO_{1.500}$	4	$Ia3$	$a = 11.152$ Å ($PrO_{1.5}$) $a = 10.728$ Å ($TbO_{1.5}$)	$a = 2a_f$	8	16
$RO_{1.714}$	7	$R\bar{3}$	$a = 6.750$ Å, $\alpha = 99°23'$ ($PrO_{1.714}$) $a = 6.509$ Å, $\alpha = 99°21'$ ($TbO_{1.714}$)	$a = a_f + \frac{1}{2}b_f - \frac{1}{2}c_f$	7/4	2
$PrO_{1.778}$	9	Triclinic	$a = 6.5$ Å $b = 8.4$ Å $c = 6.5$ Å $\alpha = 97.3°$ $\beta = 99.6°$ $\gamma = 75.0°$	$a = a_f + \frac{1}{2}b_f - \frac{1}{2}c_f$ $b = \frac{3}{2}b_f + \frac{1}{2}c_f$ $c = \frac{1}{2}a_f - \frac{1}{2}b_f + c_f$	9/4	2
$PrO_{1.800}$	10	Pn	$a = 6.7$ Å $b = 19.3$ Å $c = 15.5$ Å $\beta = 125.2°$	$a = a_f + \frac{1}{2}b_f - \frac{1}{2}c_f$ $b = \frac{5}{2}(-b_f - c_f)$ $c = 2(-b_f + c_f)$	10	8
$TbO_{1.809}$	$10\frac{1}{3}$	Triclinic	$a = 13.8$ Å $b = 16.2$ Å $c = 12.1$ Å $\alpha = 107.4°$ $\beta = 100.1°$ $\gamma = 92.2°$	$a = -\frac{1}{2}a_f + \frac{5}{2}c_f$ $b = -2a_f - 2b_f - c_f$ $c = 2a_f - b_f$	31/2	12
$RO_{1.818}$	11	Triclinic	$a = 6.5$ Å $b = 9.9$ Å $c = 6.5$ Å $\alpha = 90.0°$ $\beta = 99.6°$ $\gamma = 96.3°$	$a = a_f + \frac{1}{2}b_f - \frac{1}{2}c_f$ $b = -\frac{1}{2}a_f + \frac{3}{2}b_f + c_f$ $c = \frac{1}{2}a_f - \frac{1}{2}b_f + c_f$	11/4	2
$TbO_{1.833}$	12	Pn	$a = 6.7$ Å $b = 23.2$ Å $c = 15.5$ Å $\beta = 125.2°$	$a = a_f + \frac{1}{2}b_f - \frac{1}{2}c_f$ $b = 3(-b_f - c_f)$ $c = 2(-b_f + c_f)$	12	8
$PrO_{1.833}$	12	Pn	$a = 6.687$ Å $b = 11.602$ Å $c = 15.470$ Å $\beta = 125°15'$	$a = a_f + \frac{1}{2}b_f - \frac{1}{2}c_f$ $b = \frac{3}{2}(-b_f - c_f)$ $c = 2(-b_f + c_f)$	6	4
$RO_{2.000}$	∞	$Fm3m$	$a = 5.393$ Å (PrO_2) $a = 5.220$ Å ($TbO_{1.95}$)		1	0

[a] If a phase occurs in the PrO_x as well as in the TbO_x system R is used, otherwise the specific symbol is used.

FIGURE LEGENDS

1. The Fluorite Structure. The large circles represend metal atom positions, the triangles represent nonmetal positions and the diamonds represent the empty octahedral positions in the cubic close-packed structure.

2. Lattice Parameters for Fluorite-Related Rare Earth and Actinide Oxides.

3. Projections of the Unit Cells of Members of the Homologous Series along the Common a Axis, $[21\bar{1}]_F$.

4. Arrangement of Vacancy Pairs along the a axis, $[21\bar{1}]_F$ Common to Members of the Homologous Series.

5. Crystal Structure Image of $Tb_{11}O_{20}$. Dark field, optically enhanced.

6. The Possible Structures of Delta ($Pr_{11}O_{20}$) Projected down $[211]_F$.

7. Projections of the Ideal Atom Positions of Pr_7O_{12} down a) the $[111]_F$ axis where the line intersections, filled triangles and empty triangles represent columns of metal and nonmetal sites at relative intervals of $\frac{1}{12}[111]_F$ to each other. The columns of nonmetal vacancies and six-coordinated metal atoms are indicated by filled circles and b) the $[211]_F$ axis where metal atom sites are marked with a plus sign, the nonmetal sites are marked by a multiplication sign, nonmetal vacancies are marked with a square and filled circles again indicate columns of six-coordinated metal atoms. MO_8 cubes are also outlined to facilitate interpretation.

8. Calculated Images of Pr_7O_{12} and $Zr_3Sc_4O_{12}$. The type of scattering factors and the defect of focus are shown at the bottom while the number of slices ($\sim$ 6.75Å per slice) are shown at the left.

9. Observed $\langle 100 \rangle_7$ Crystal Structure Images of Pr_7O_{12} and $Zr_3Sc_4O_{12}$: a) typical image of Pr_7O_{12}; b) thick-crystal image of Pr_7O_{12} and c) thin-crystal image of $Zr_3Sc_4O_{12}$ showing vacancy arrangement.

10. Observed $\langle 111 \rangle_7$ Images of Pr_7O_{12} and $Zr_3Sc_4O_{12}$: a) typical image, b) two twin orientations of $Zr_3Sc_4O_{12}$ with a region of C-type oxide between.

11. $\langle 111 \rangle_{12}$ Crystal Structure Images of Beta.

12. Diagrammatic Representations of the Proposed Structures of the Beta Phase. a) Model with symmetry P1. b) Model with symmetry Pm. Indices refer to fluorite subcell.

13. Calculated Images of Beta Phase with the Defect of Focus and the Thickness of the Crystal Indicated.

14. Crystal Structure Image from $\langle 100 \rangle_{12}$ showing Image Variations which may correspond to Domains of each of the Proposed Polymorphs of Beta.

15. Crystal Structure Image of Beta from a $\langle 100 \rangle_{12}$ Zone showing apparent stacking faults.

16. Crystal Structure Image from a $\langle 100 \rangle_{10}$ Zone of Epsilon.

17. $\langle 211 \rangle_F$ Crystal Structure Image of the Zeta Phase.

18. (a) Crystal Structure Image from $\langle 100 \rangle_9$ showing intergrowth with Iota. (b) $\langle 111 \rangle_F$ Crystal Structure Image showing a domain of Pr_7O_{12} in a Crystal which is largely Sigma Phase.

19. Domains of Sc_2O_3 in a Matrix of $Zr_3Sc_4O_{12}$ as seen in $\langle 111 \rangle_F$ Images.

20. Disorder Evident in $\langle 111 \rangle_7$ Images of $Zr_3Sc_4O_{12}$.

21. Intergrowth in Pr_nO_{2n-2} $[21\bar{1}]_F$ Zone.

22. Schematic Representation of the Intergrowth Phases shown in Figure 21.

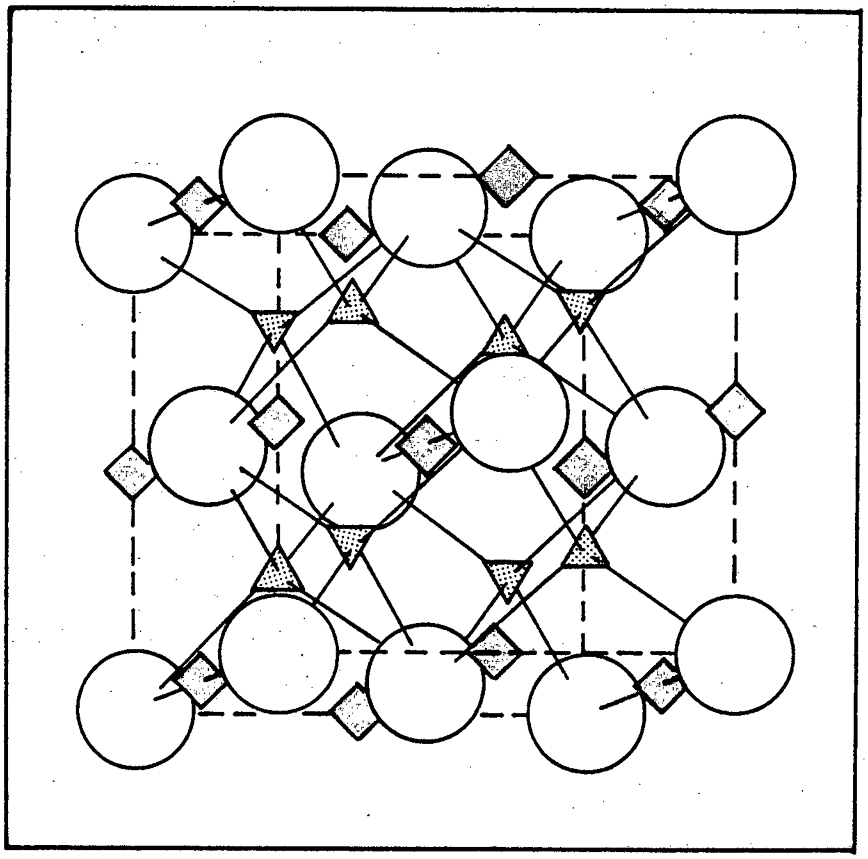

Figure 1. The Fluorite Structure. The large circles represend metal atom positions, the triangles represent nonmetal positions and the diamonds represent the empty octahedral positions in the cubic close-packed structure.

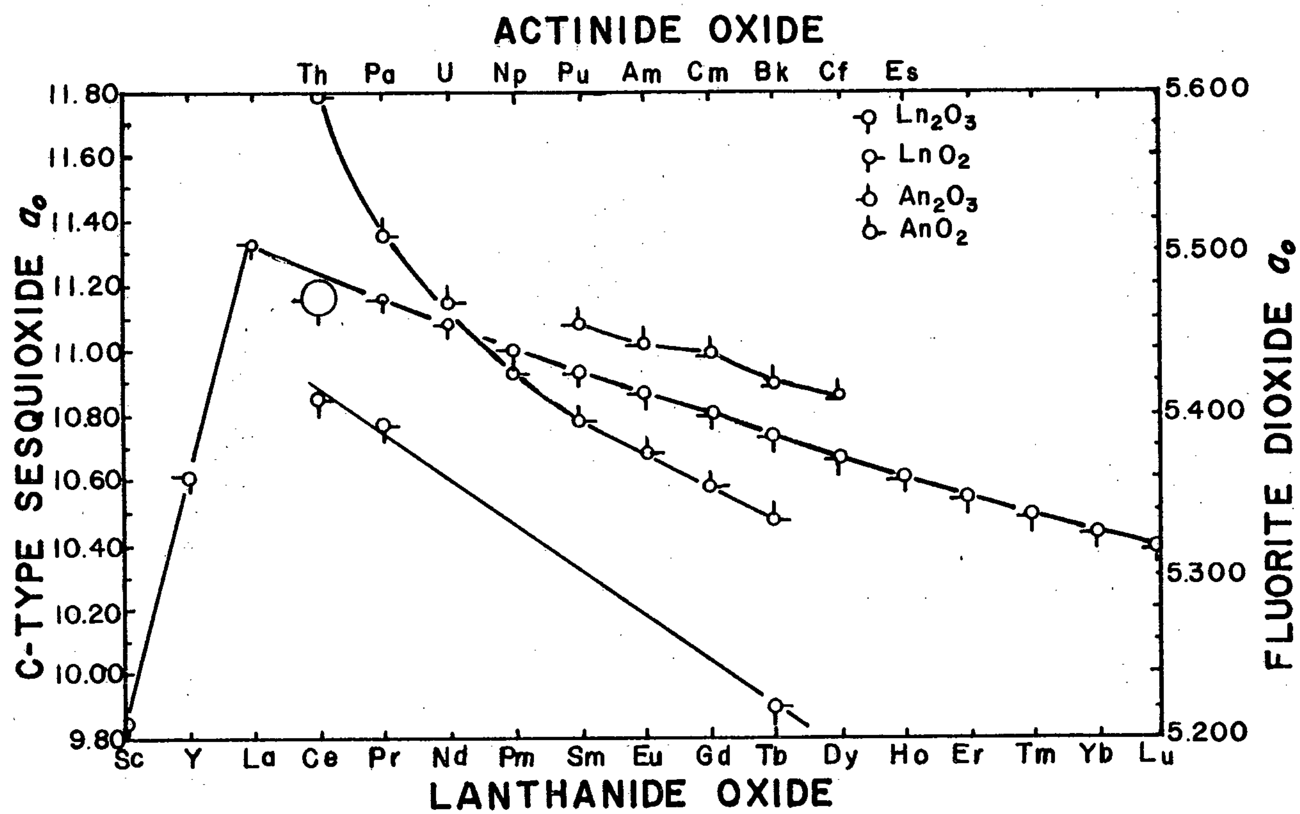

Figure 2. Lattice Parameters for Fluorite-Related Rare Earth and Actinide Oxides.

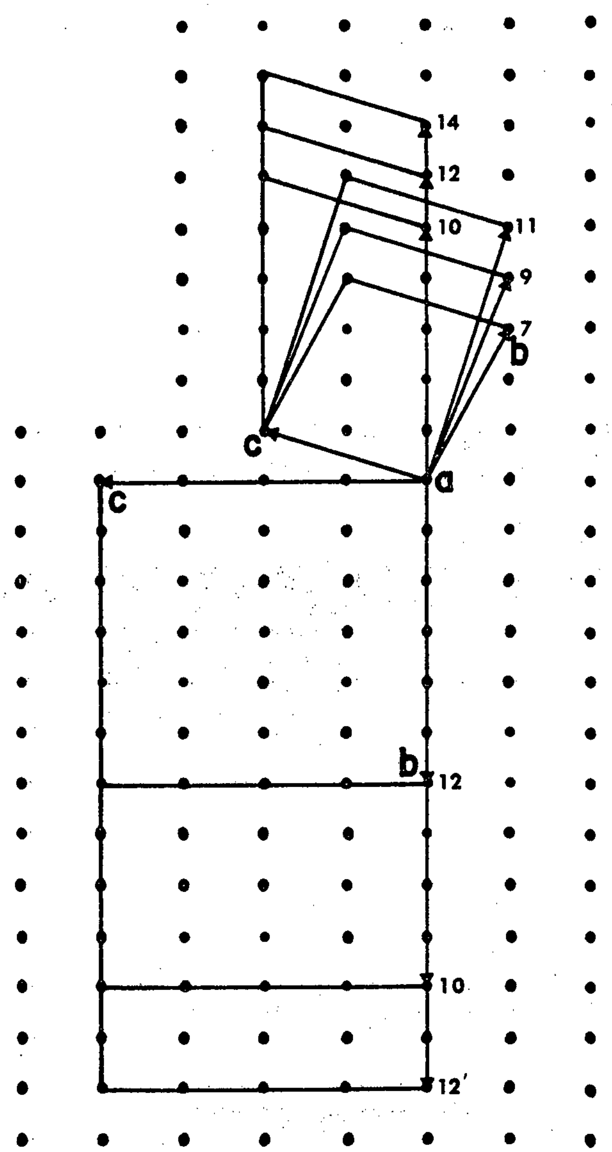

Figure 3. Projections of the Unit Cells of Members of the Homologous Series along the Common $\underline{a}$ Axis, $[21\bar{1}]_F$.

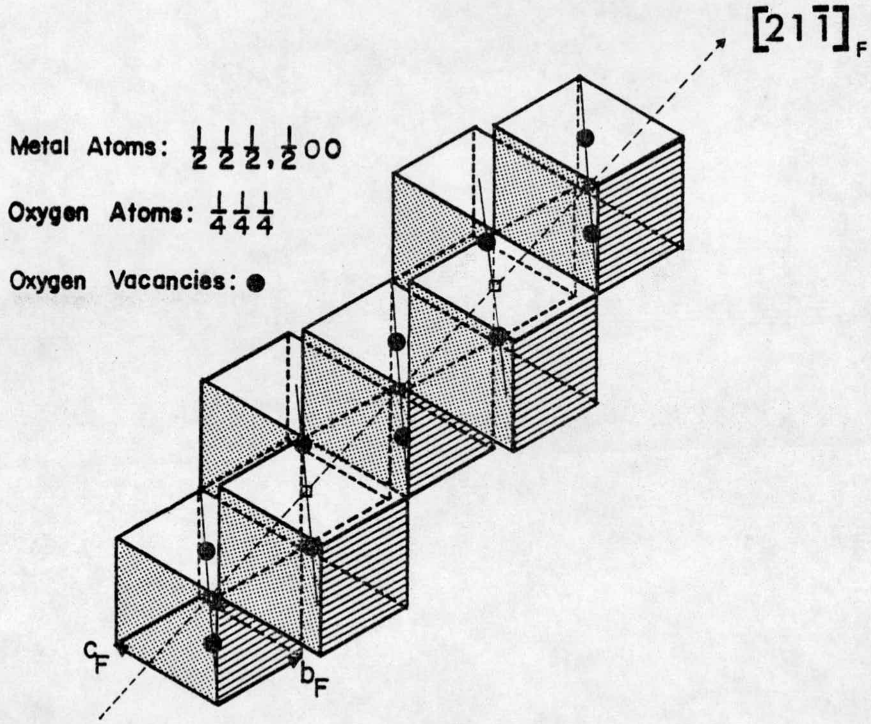

Figure 4. Arrangement of Vacancy Pairs along the a axis, $[21\bar{1}]_F$ Common to Members of the Homologous Series.

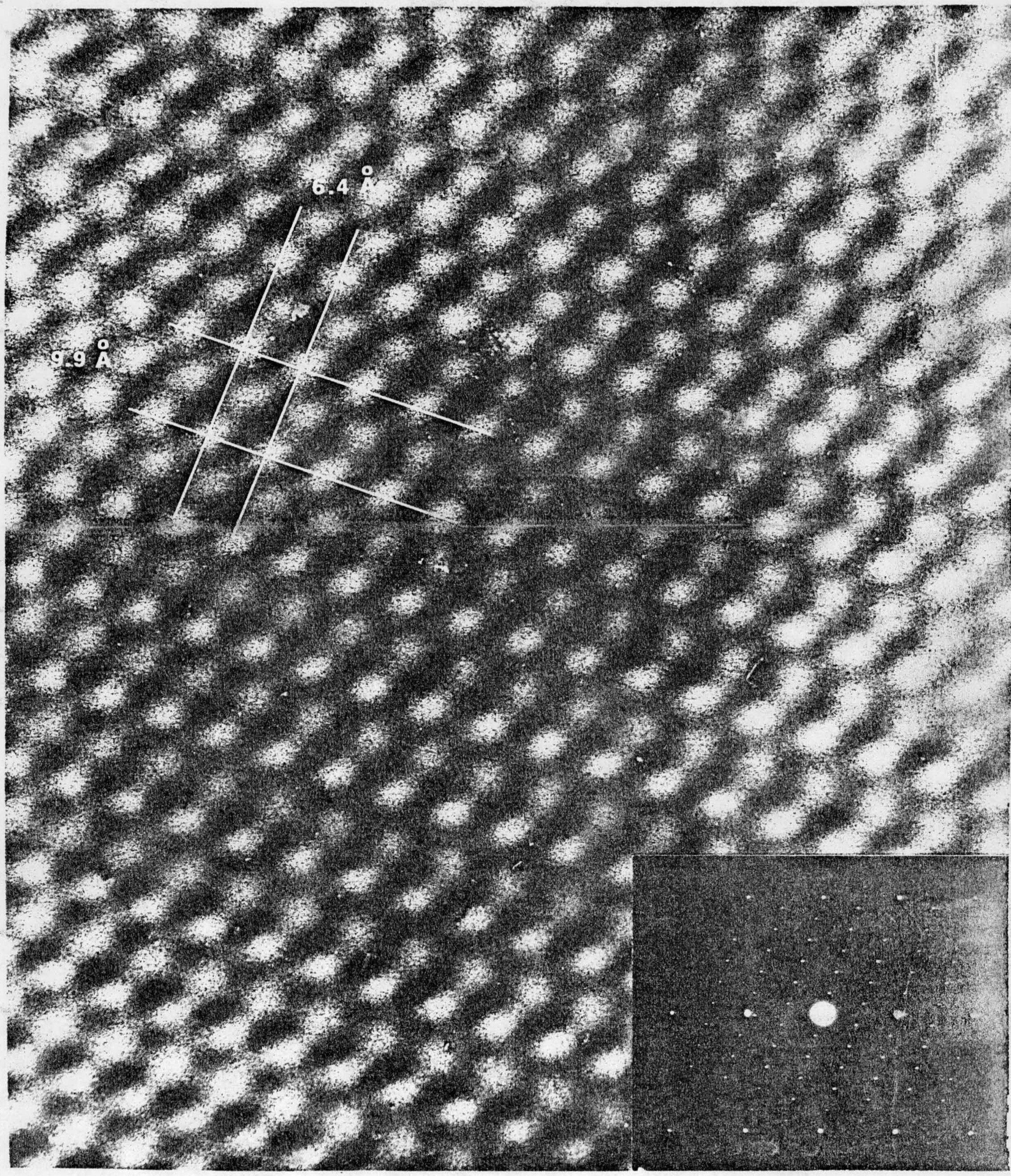

Figure 5. Crystal Structure Image of $Tb_{11}O_{20}$. Dark field, optically enhanced.

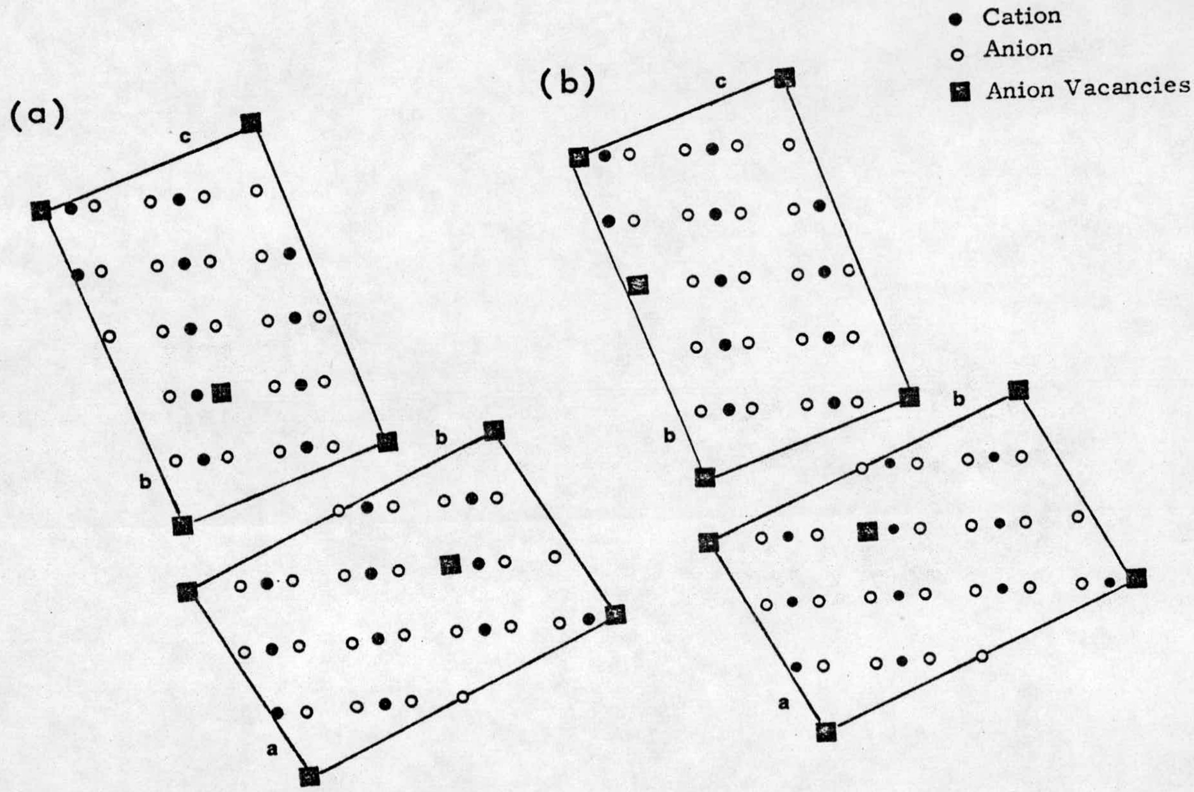

Figure 6. The Possible Structures of Delta ($Pr_{11}O_{20}$) Projected down $[211]_F$.

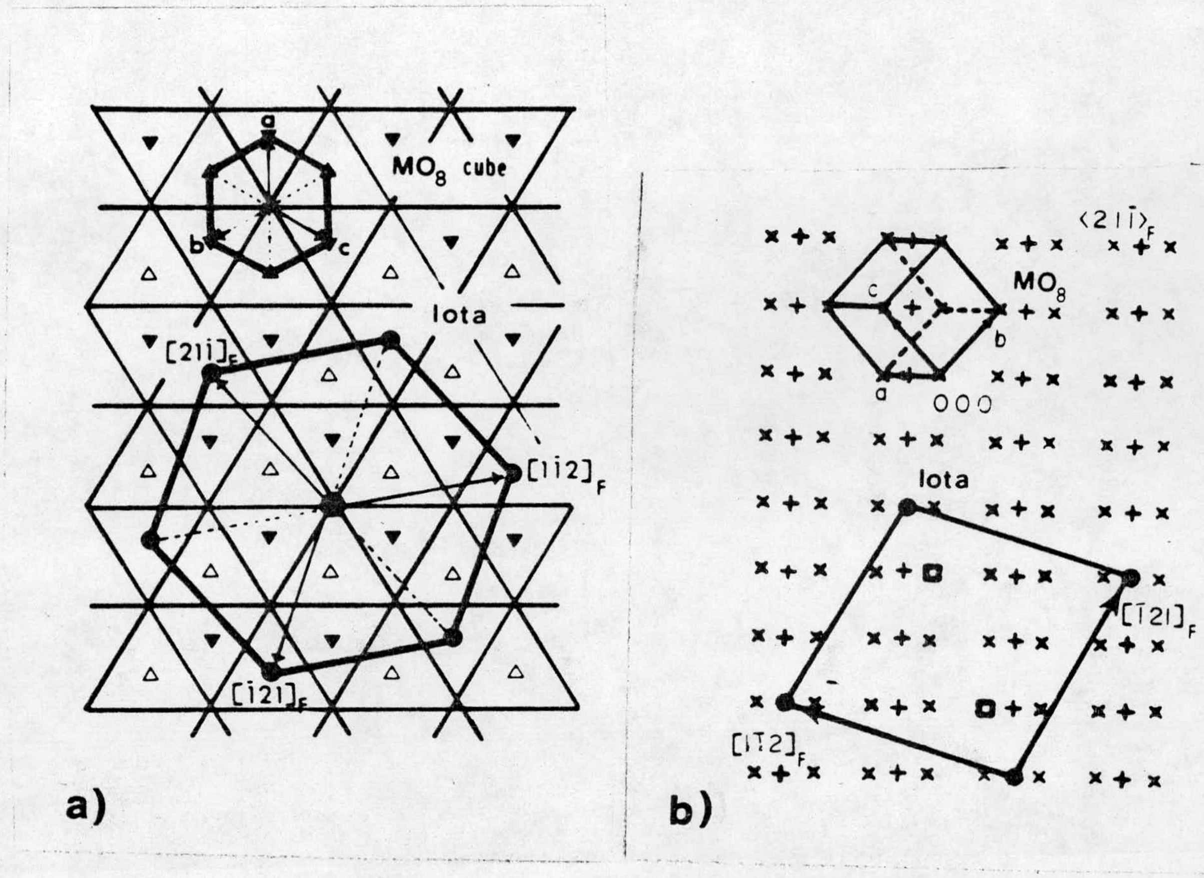

Figure 7. Projections of the Ideal Atom Positions of Pr_7O_{12} down a) the $[111]_F$ axis where the line intersections, filled triangles and empty triangles represent columns of metal and nonmetal sites at relative intervals of $\frac{1}{12}[111]_F$ to each other. The columns of nonmetal vacancies and six-coordinated metal atoms are indicated by filled circles and b) the $[211]_F$ axis where metal atom sites are marked with a plus sign, the nonmetal sites are marked by a multiplication sign, nonmetal vacancies are marked with a square and filled circles again indicate columns of six-coordinated metal atoms. MO_8 cubes are also outlined to facilitate interpretation.

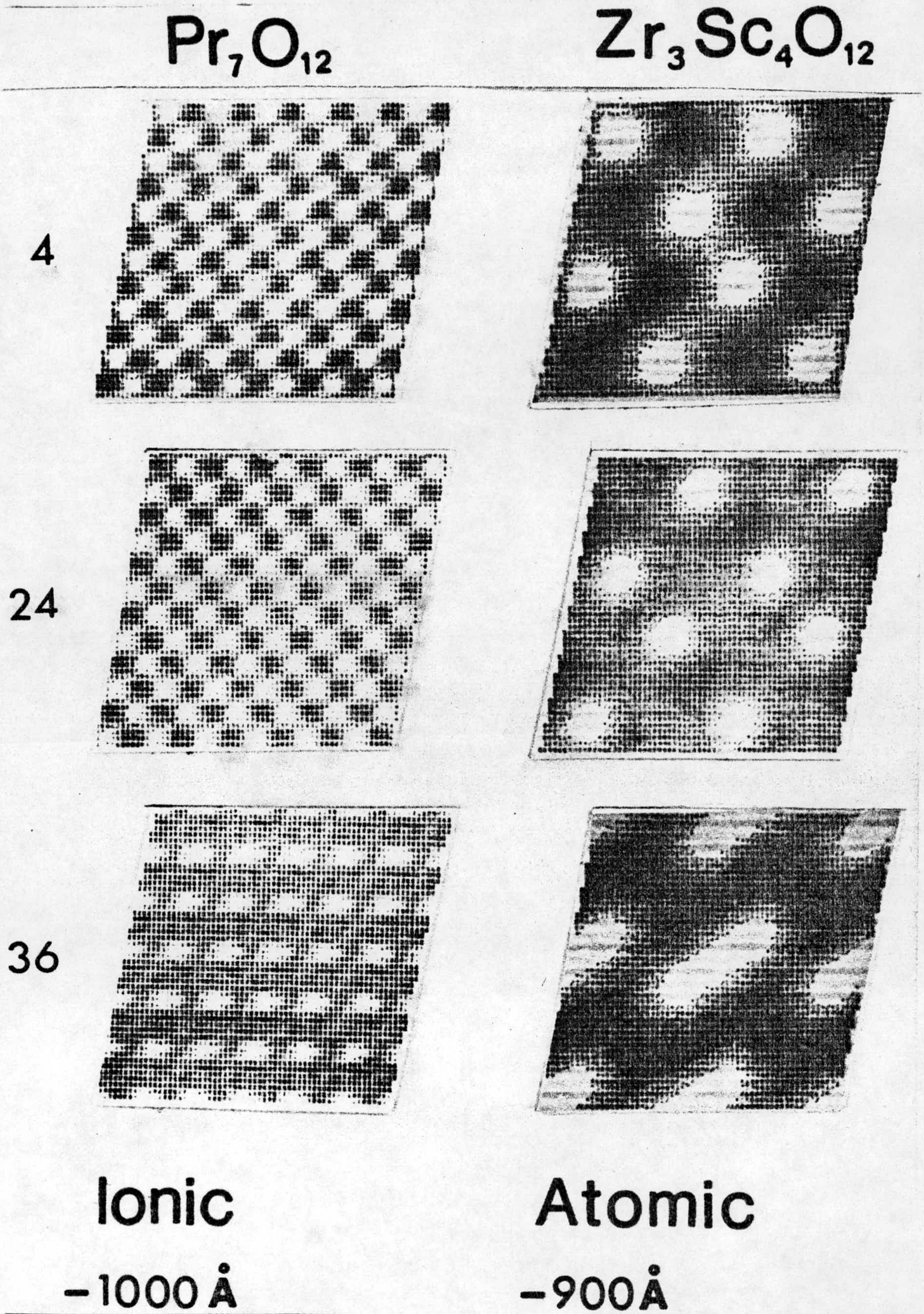

Figure 8. Calculated Images of Pr_7O_{12} and $Zr_3Sc_4O_{12}$. The type of scattering factors and the defect of focus are shown at the bottom while the number of slices (~ 6.75Å per slice) are shown at the left.

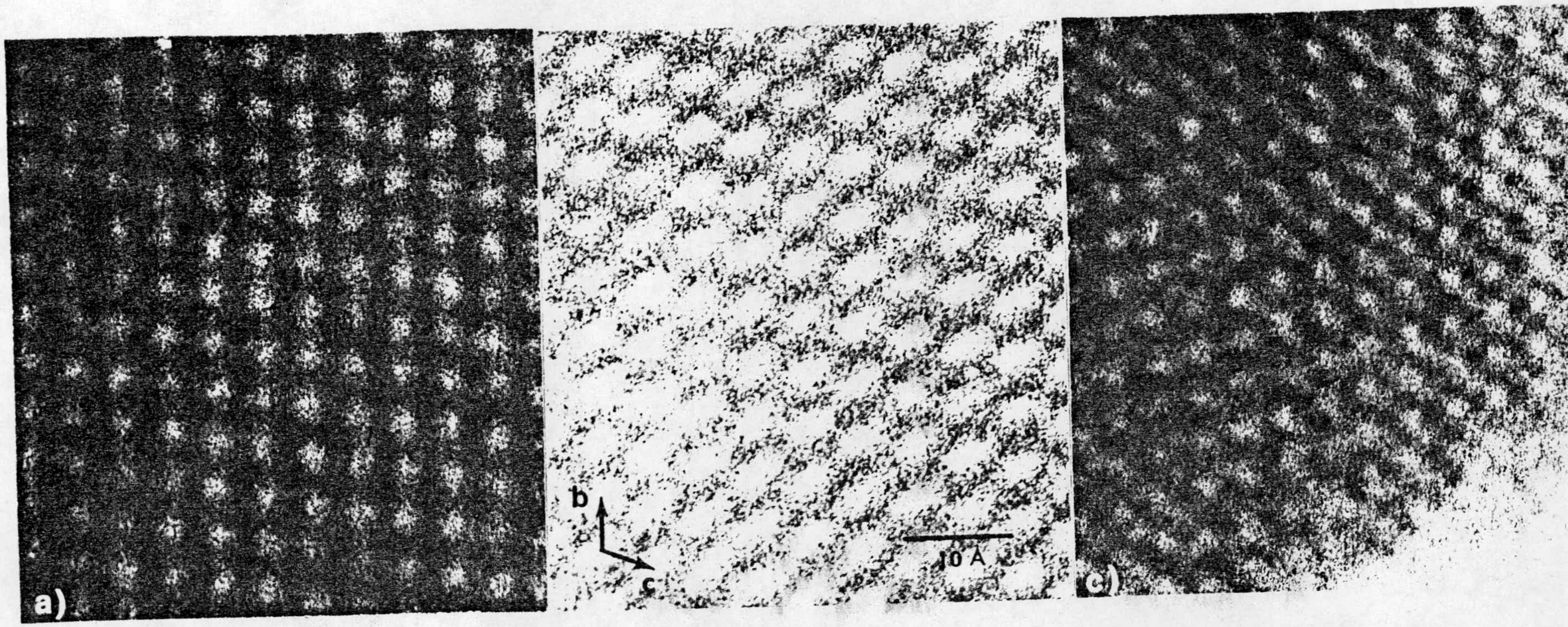

Figure 9. Observed $\langle 100 \rangle_7$ Crystal Structure Images of Pr_7O_{12} and $Zr_3Sc_4O_{12}$: a) typical image of Pr_7O_{12}; b) thick-crystal image of Pr_7O_{12} and c) thin-crystal image of $Zr_3Sc_4O_{12}$ showing vacancy arrangement.

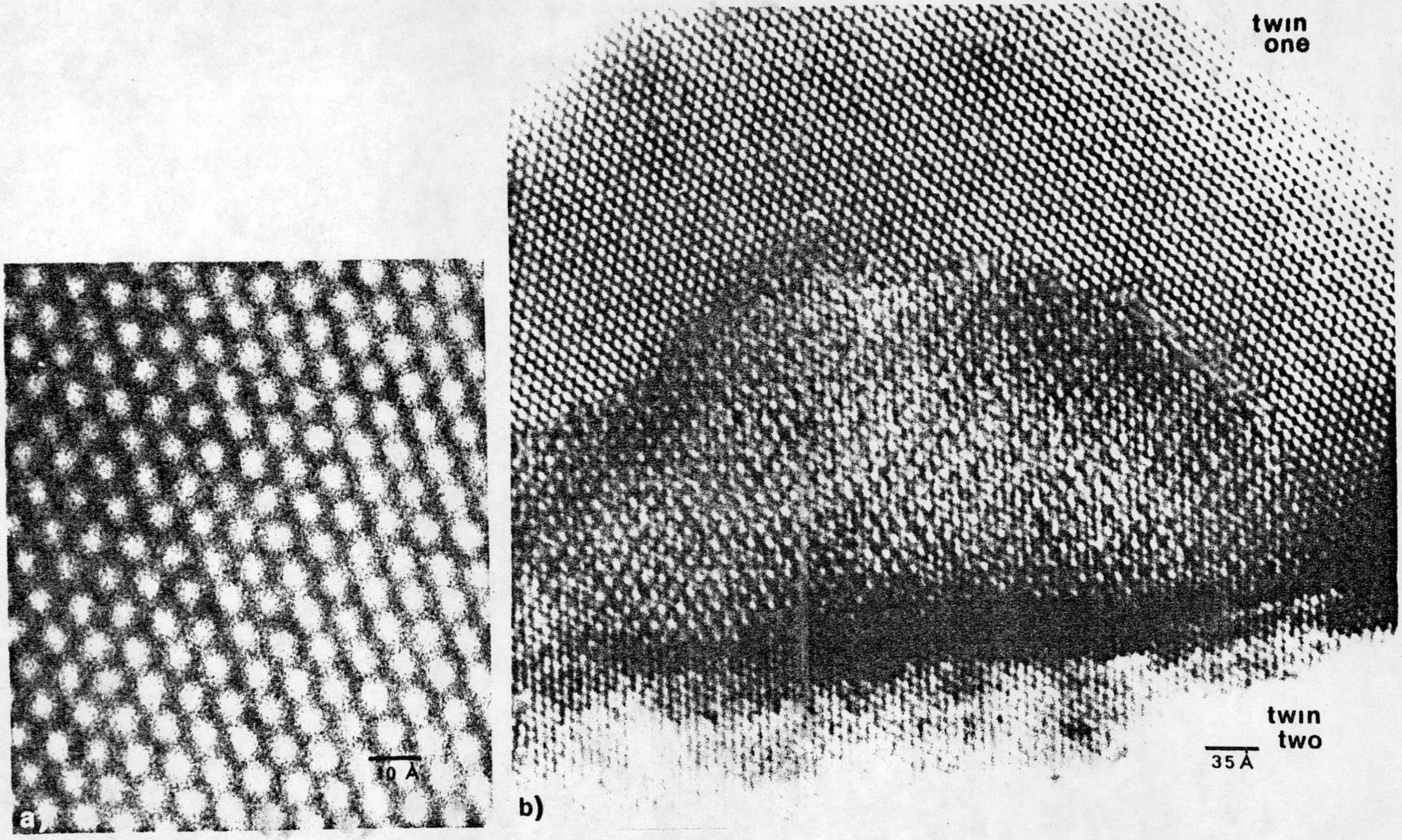

Figure 10. Observed $\langle 111 \rangle_7$ Images of Pr_7O_{12} and $Zr_3Sc_4O_{12}$:
a) typical image, b) two twin orientations of $Zr_3Sc_4O_{12}$
with a region of C-type oxide between.

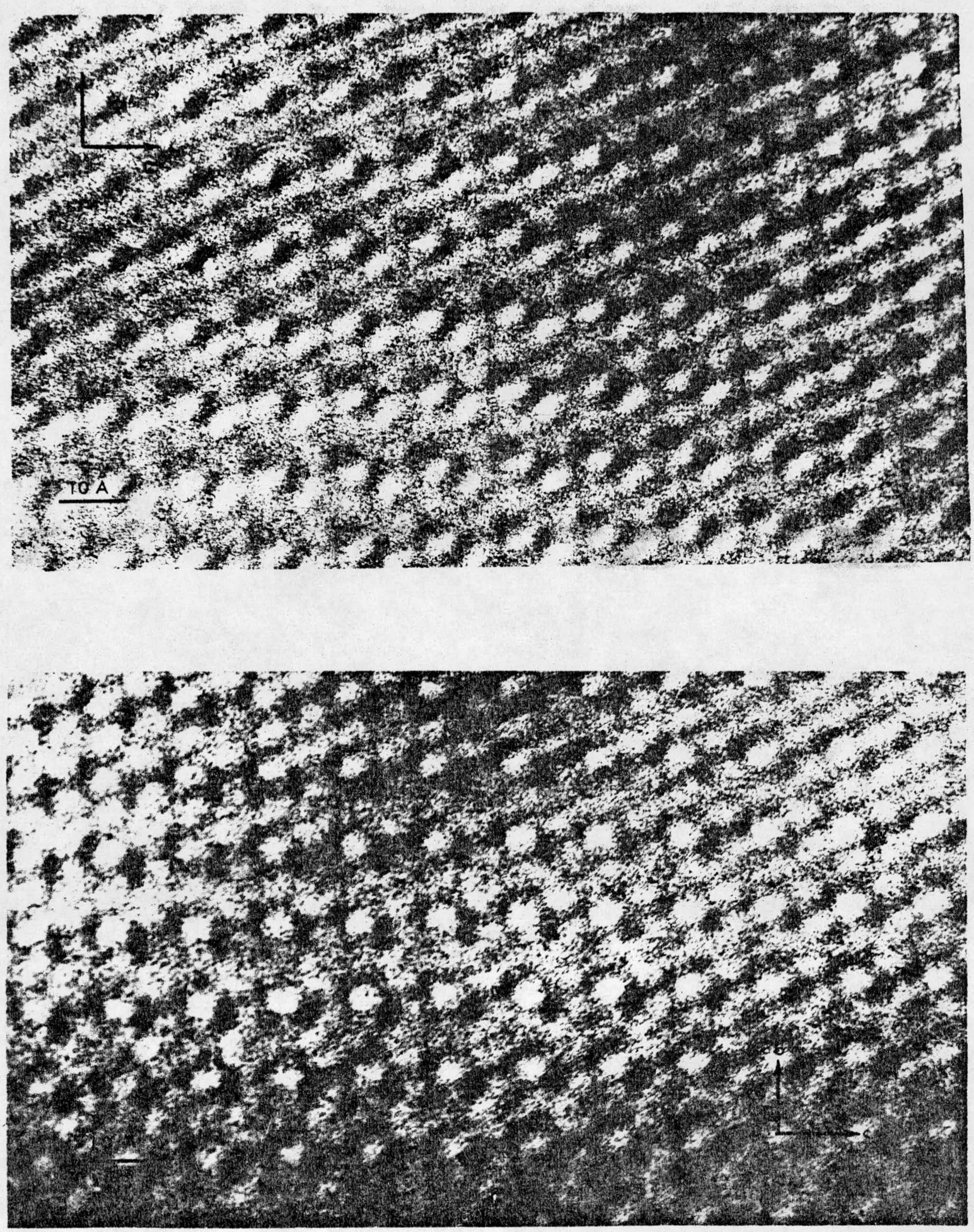

Figure 11. $\langle 111 \rangle_{12}$ Crystal Structure Images of Beta.

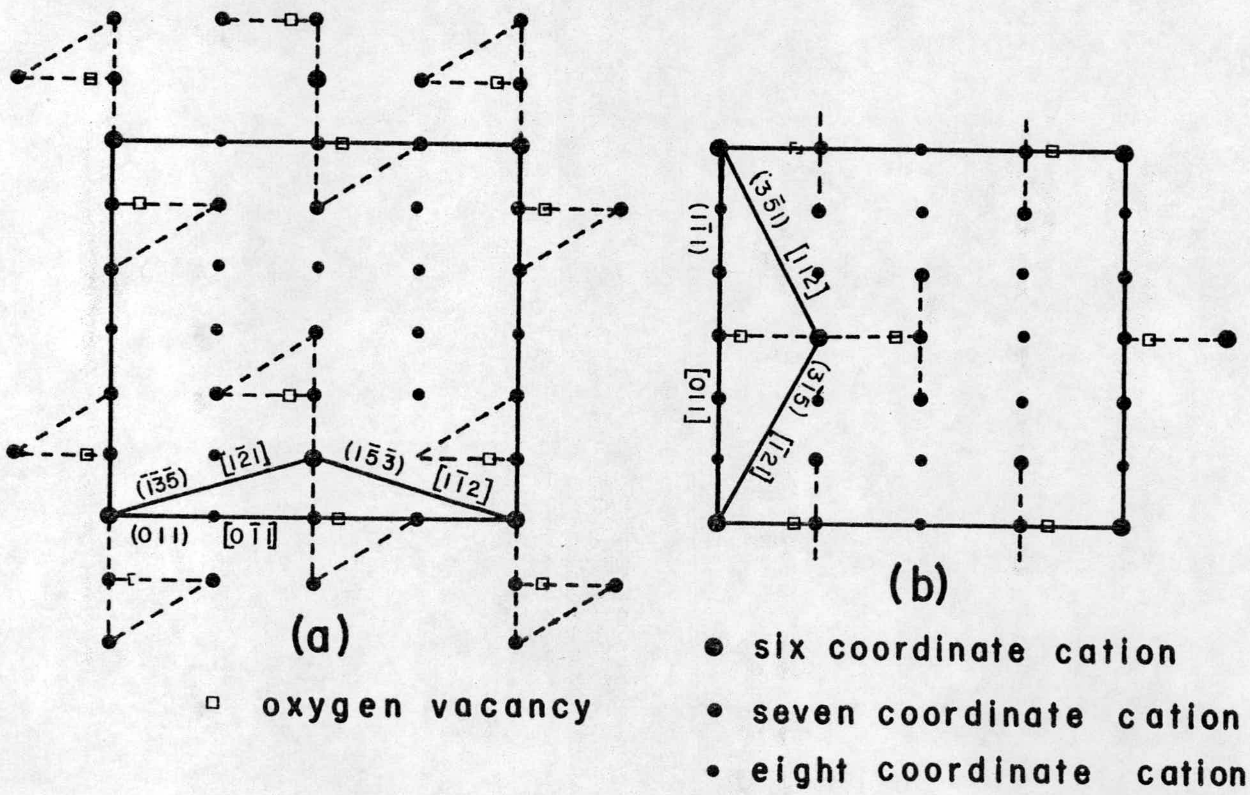

Figure 12. Diagrammatic Representations of the Proposed Structures of the Beta Phase. a) Model with symmetry P1. b) Model with symmetry Pm. Indices refer to fluorite subcell.

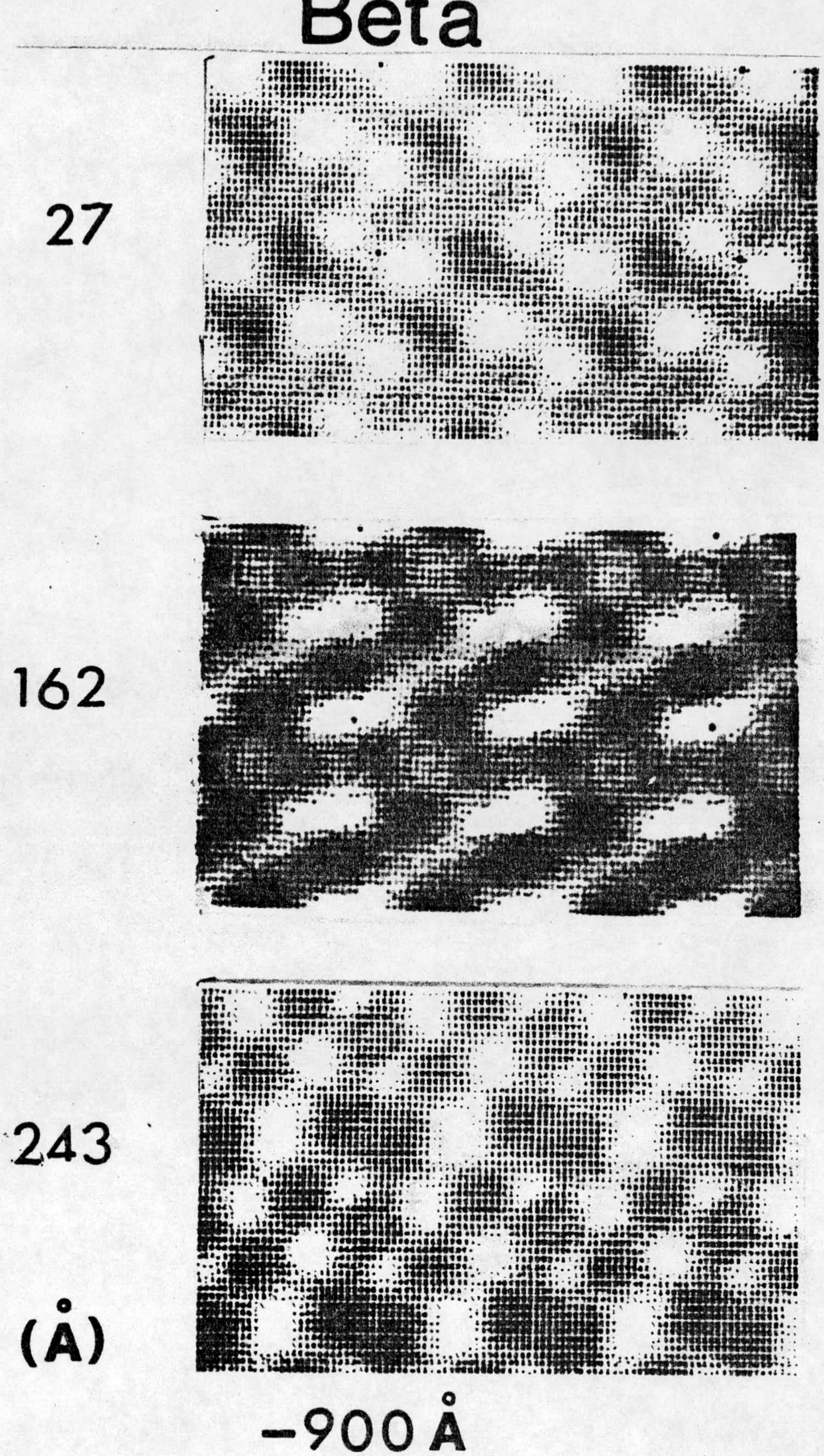

Figure 13. Calculated Images of Beta Phase with the Defect of Focus and the Thickness of the Crystal Indicated.

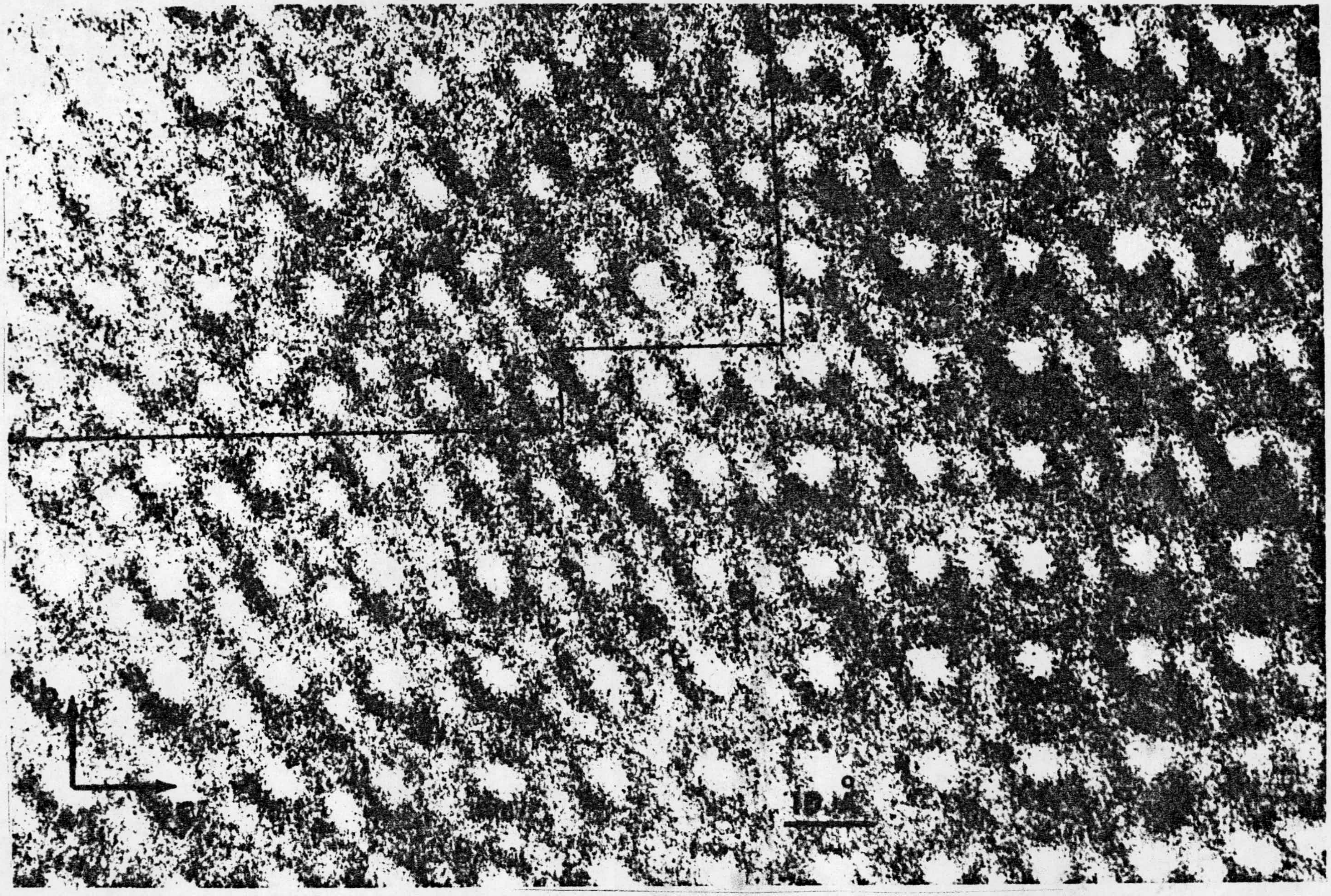

Figure 14. Crystal Structure Image from $\langle 100 \rangle_{1\,2}$ showing Image Variations which may correspond to Domains of each of the Proposed Polymorphs of Beta.

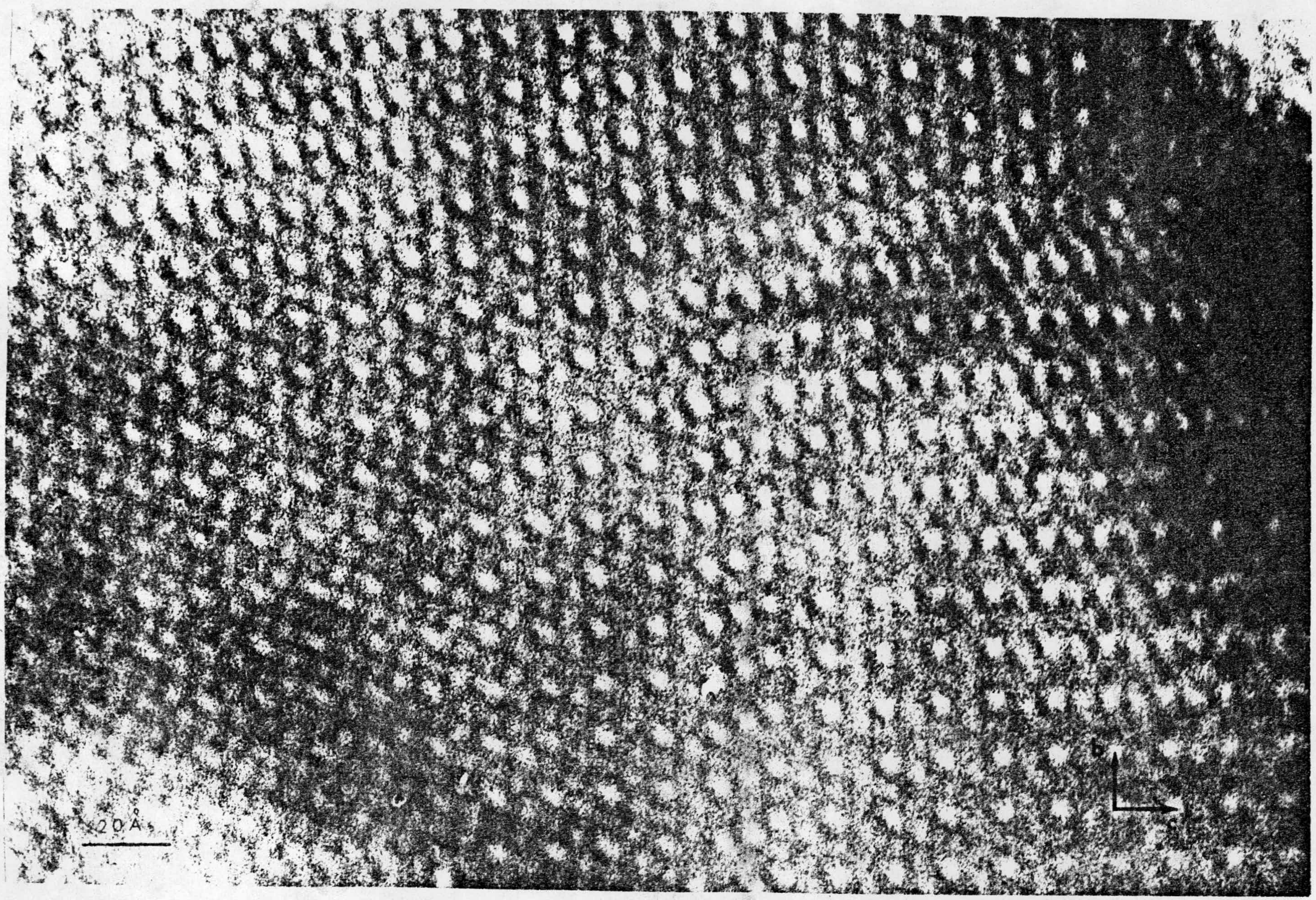

Figure 15. Crystal Structure Image of Beta from a $\langle 100 \rangle_{12}$ Zone showing apparent stacking faults.

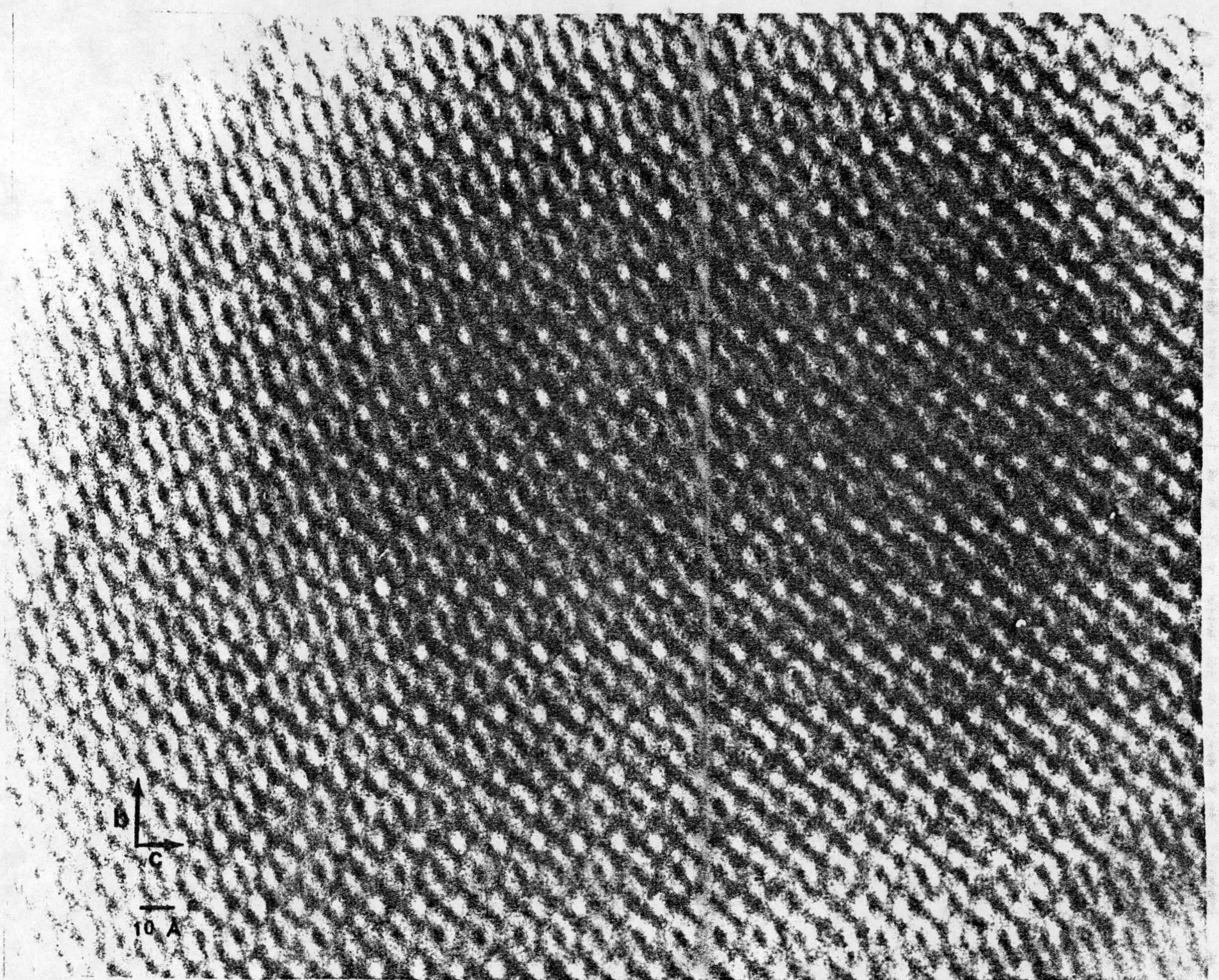

Figure 16. Crystal Structure Image from a $\langle 100 \rangle_{10}$ Zone of Epsilon.

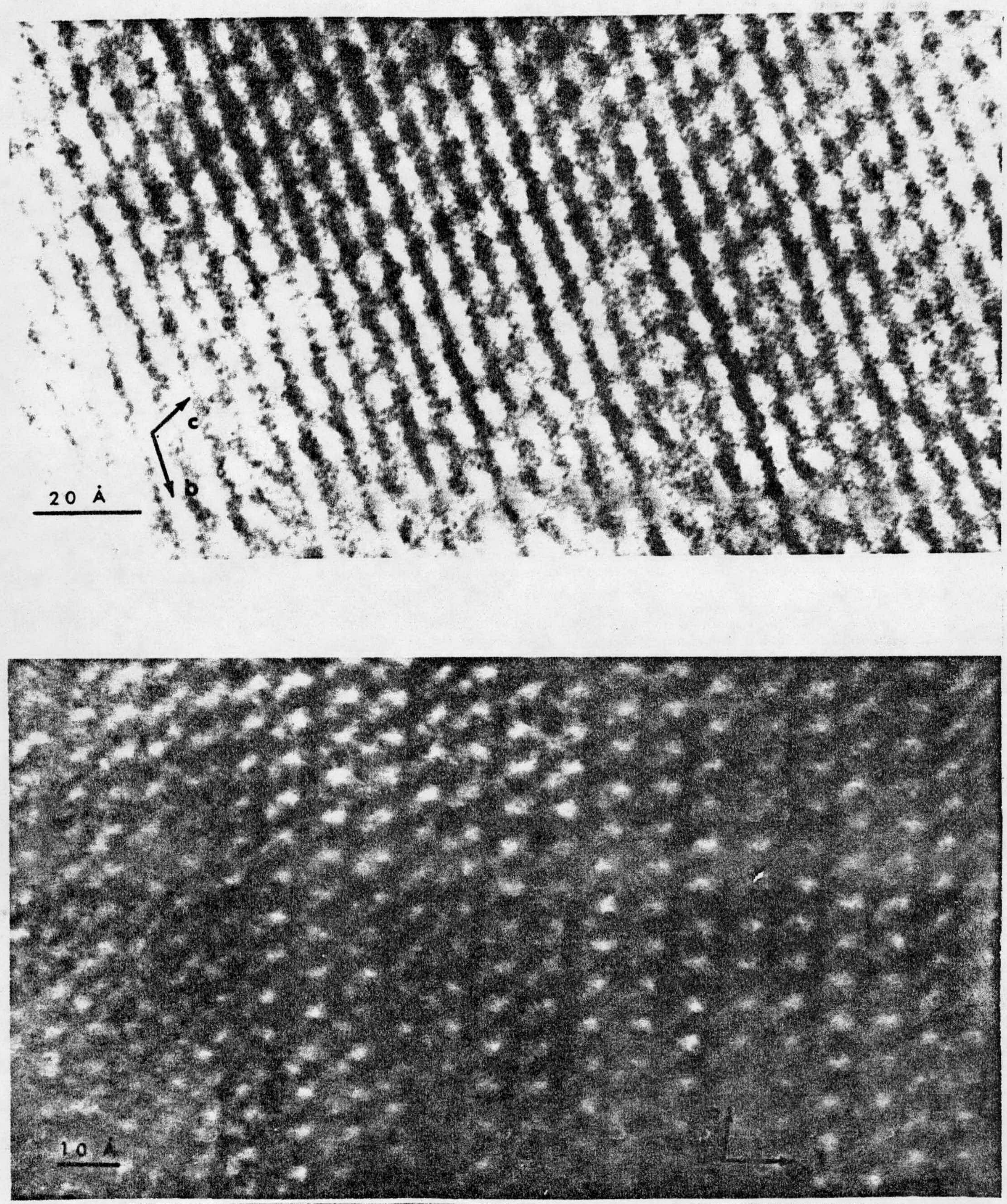

Figure 17. $\langle 211 \rangle_F$ Crystal Structure Image of the Zeta Phase.

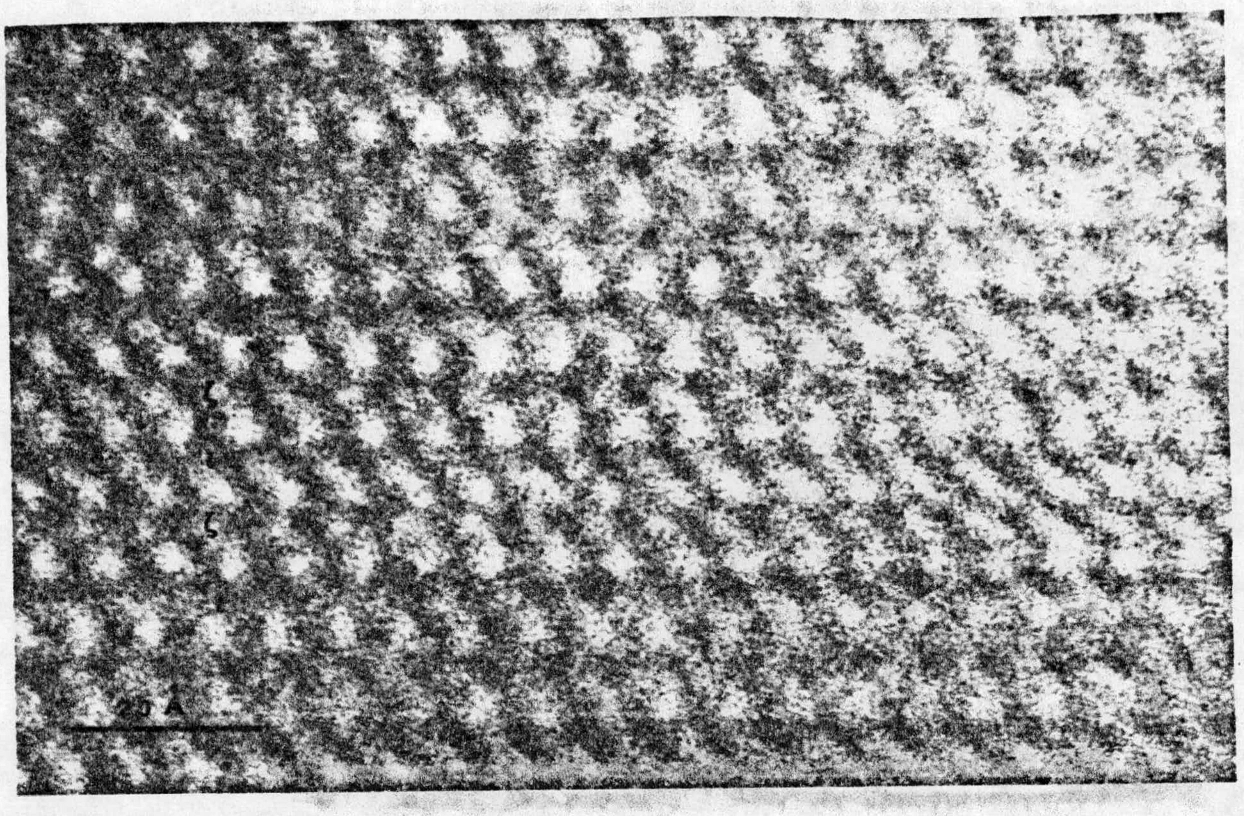

(a)

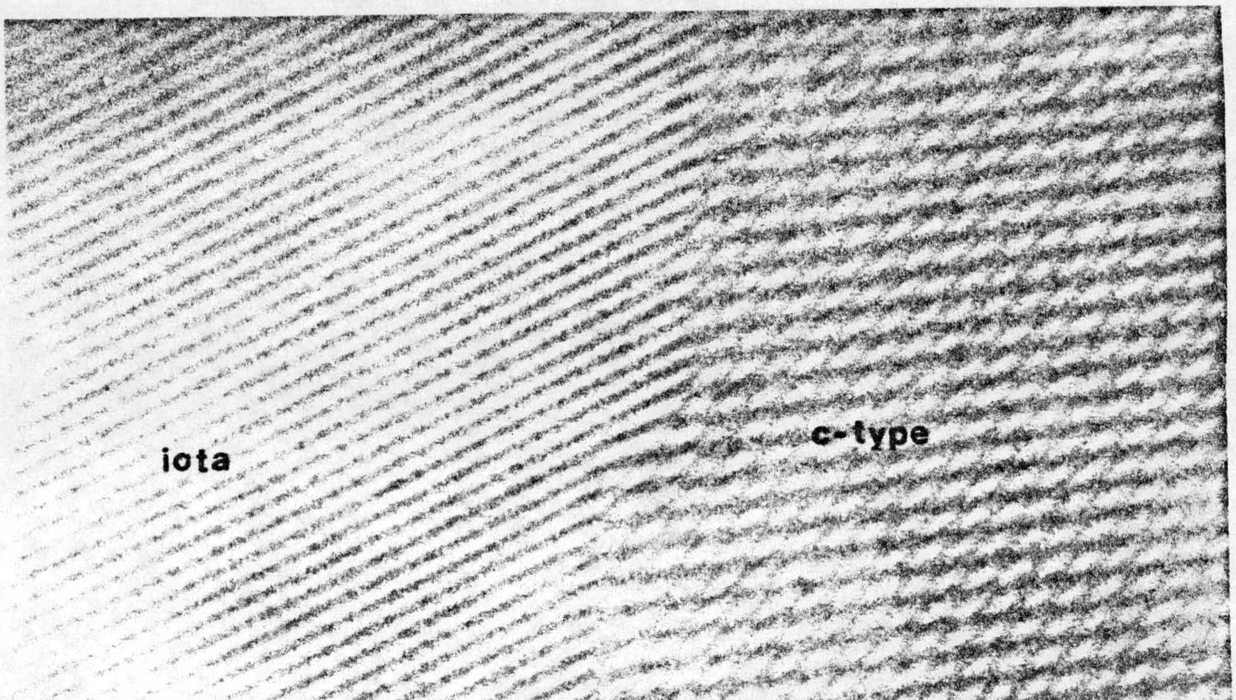

(b)

Figure 18. (a) Crystal Structure Image from $\langle 100 \rangle_9$ showing intergrowth with Iota. (b) $\langle 111 \rangle_F$ Crystal Structure Image showing a domain of Pr_7O_{12} in a Crystal which is largely Sigma Phase.

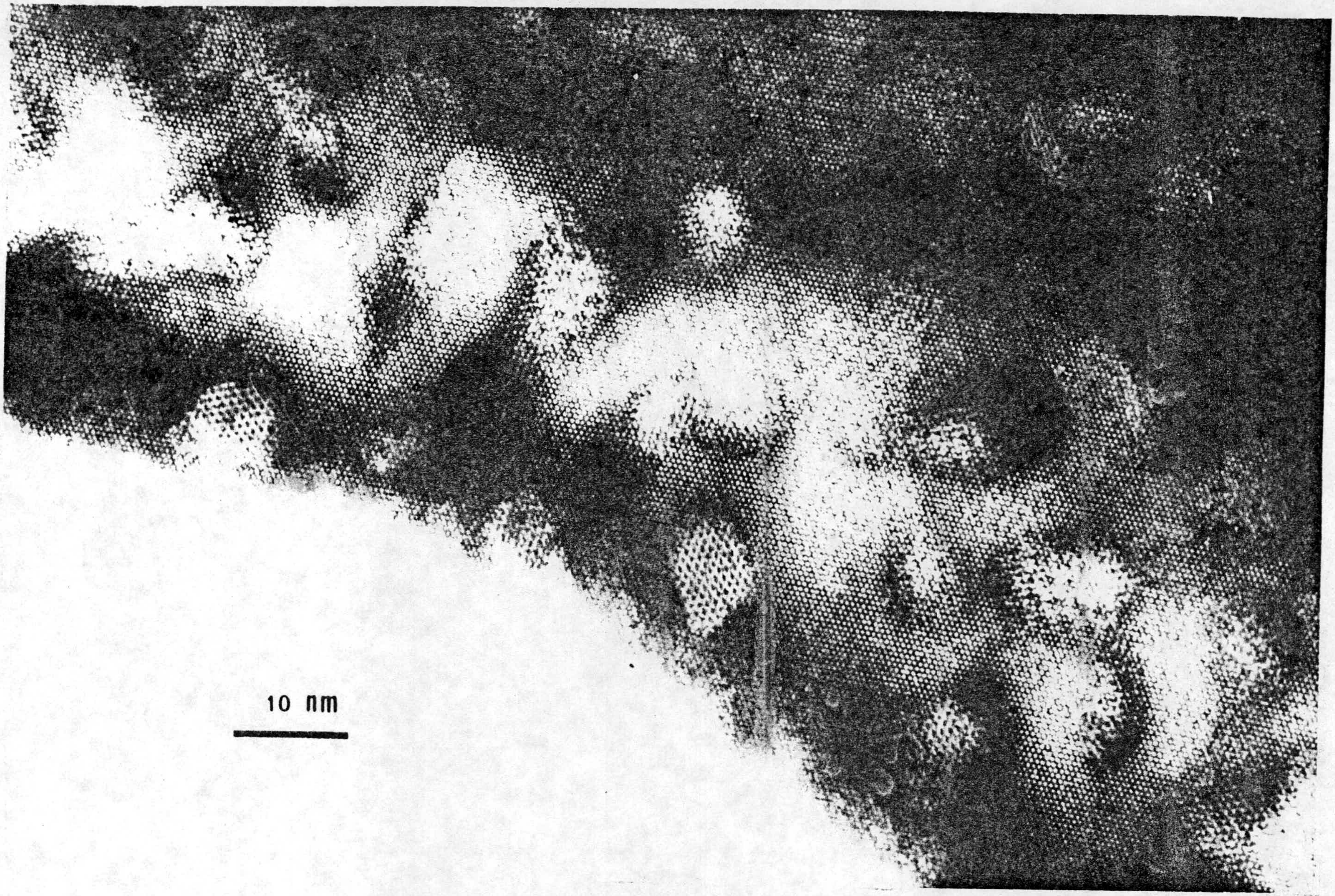

Figure 19. Domains of Sc_2O_3 in a Matrix of $Zr_3Sc_4O_{12}$ as seen in $\langle 111 \rangle_F$ Images.

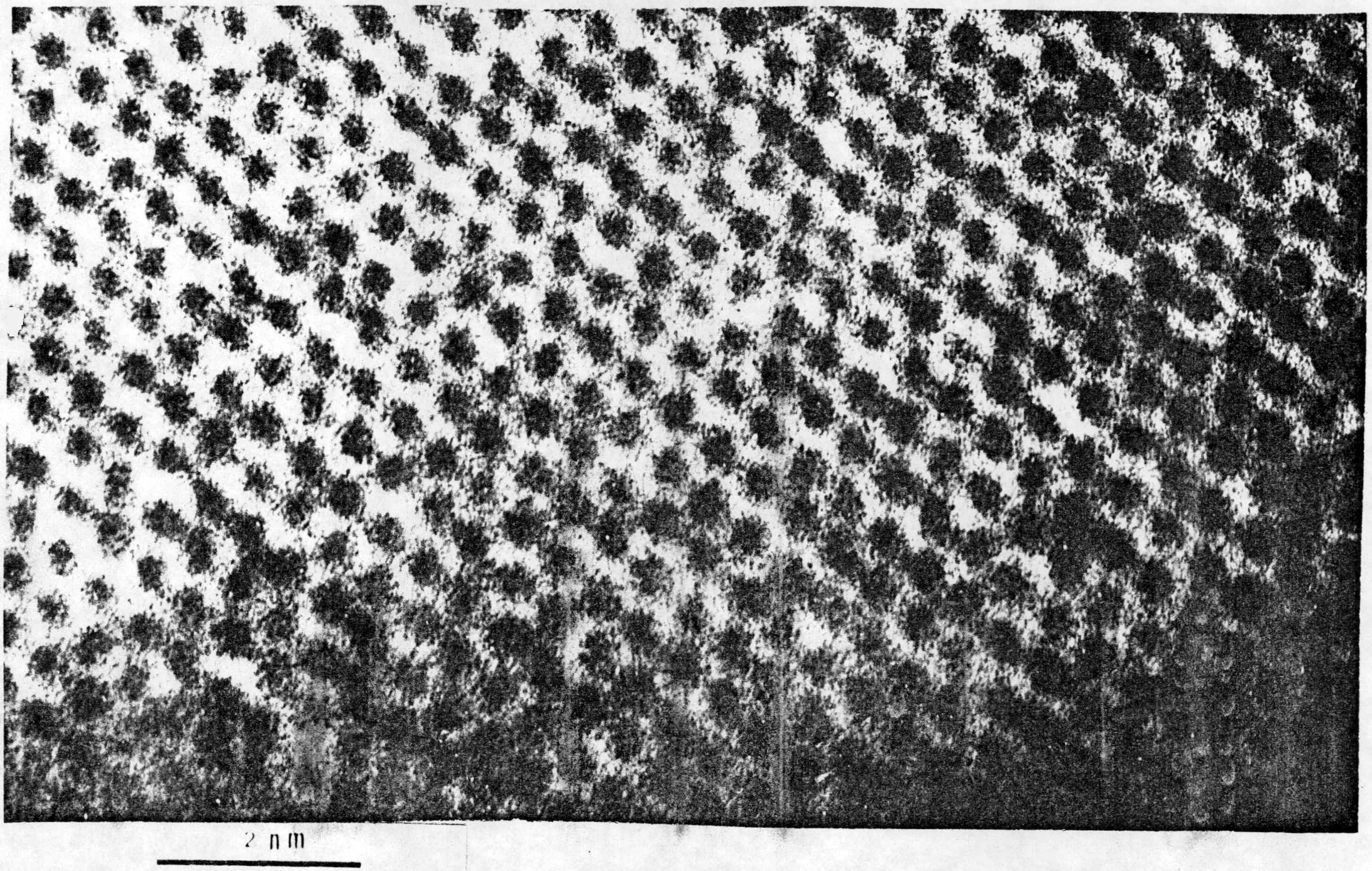

Figure 20. Disorder Evident in $\langle 111 \rangle_7$ Images of $Zr_3Sc_4O_{12}$.

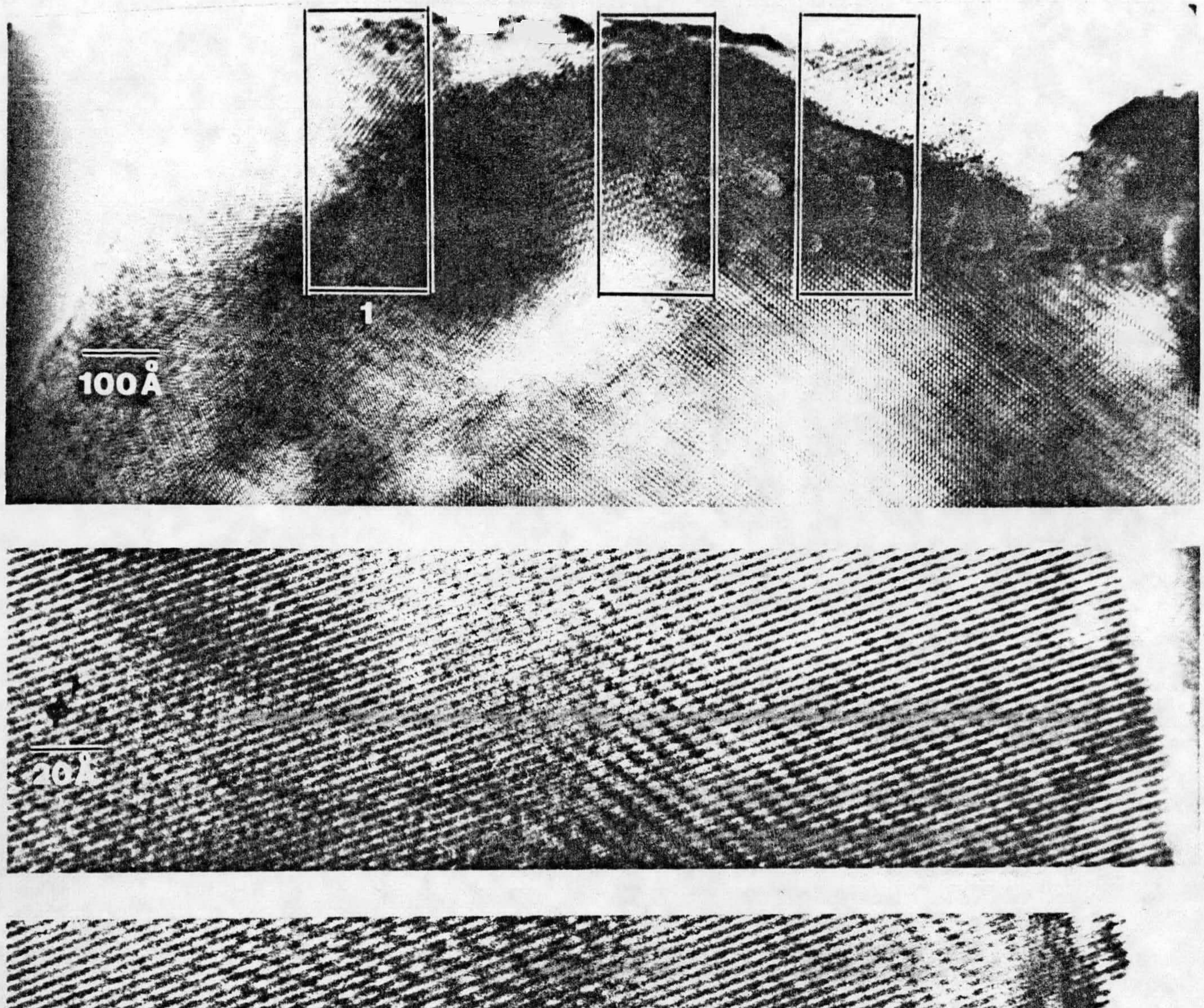

Figure 21. Intergrowth in Pr_nO_{2n-2} $[21\bar{1}]_F$ Zone.

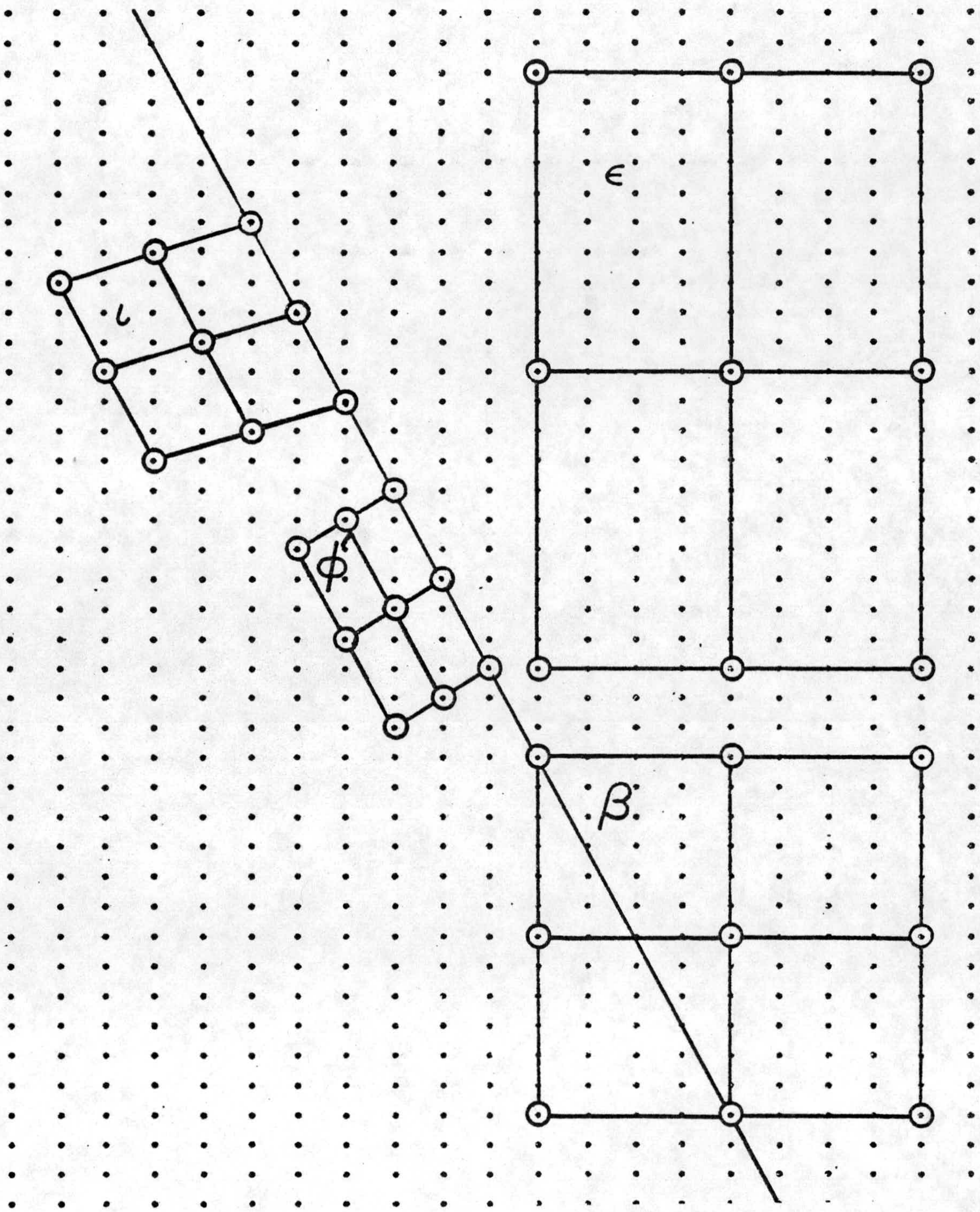

Figure 22. Schematic Representation of the Intergrowth Phases shown in Figure 21.

III

AN INTERACTIVE CRYSTAL STRUCTURE IMAGE CALCULATION SYSTEM

INTRODUCTION

During the past several years high resolution electron microscopy has been used to investigate many of the ordered intermediate phases belonging to the fluorite-related homologous series R_nO_{2n-2}. Kunzmann and Eyring[1] have discussed the application of this technique for obtaining the unit cells and possibly the structures of those ordered phases. Skarnulis[2] has shown that the use of n-beam dynamical image calculations can provide a method by which proposed models for defect structures can be tested by comparing the calculated crystal structure images with those actually obtained in the electron microscope.

A major difficulty in the interpretation of crystal structure images of the fluorite-related phases is that experimental images obtained so far do not represent the projected crystal potential. Hence there is not a one-to-one correspondence between spots in the image and atoms (or vacancies). Also, calculations on these materials have shown that the image changes markedly with crystal thickness. For thin crystals (less than ~ 75Å) the number of white spots and their arrangement corresponds to that of the vacancy model upon which the calculation was based. As the thickness of the crystal increases the correspondence between the image and vacancy arrangement vanishes. Thus the process of determining the crystal structure of the defect fluorite phases is basicly one of trial and error. Furthermore, the determination of the best match of the calculated and experimental image is at this time entirely subjective.

The process by which electron microscopic crystal structure images are employed to test proposed structural models involves calculations for a number of values of image parameters such as crystal thickness, underfocus and aperture size for each model. The best situation for these calculations would be an interactive system in which the image parameters could be varied and the effects on the image rapidly computed and displayed. The process of matching the calculated images with the experimental image could be improved by digitizing the contrast on the microscope plates in order that a numerical comparison with calculated images can be facilitated. It is hoped that the interactive image calculation system described here will accomplish these objectives.

interactive operating system will be written directly in assembler language.

In order to create assembler programs on the Nova additional software is necessary. A Data General cross assembler (FORTRAN V) was acquired and debugged. The cross assembler will enable Data General mnemonics to be translated into machine code thus generating an absolute element on the system. The cross assembler will run on the University's UNIVAC 1110 computer. The output of the cross assembler is in either absolute or relocatable form. Since the design of a system with the size and complexity needed for the image calculations would be very difficult and time-consuming, a relocatable loader was written. This program, written in UNIVAC assembler, uses the relocatable output from the cross assembler to generate a NOVA core-image. The core-image could be loaded into our system by dumping it on 9-track magnetic tape or by a direct data transfer utilizing a modem setup. This method will enable all of the assembler programs to be stored, assembled and mapped on the UNIVAC providing maximum speed and flexibility. The cross-assembler and relocatable loader are operational.

The executive system will control the loading of programs and the manipulation of save-files, scratch-files, image-files and utilities from the magnetic tape unit. The image calculations will be done as extensively as possible in core in order to minimize I/O time. The executive system would allow the names of all of the programs in the library to be displayed on the Tektronics graphics terminal. The program to be run would be selected by the cross-hair cursor and automatically loaded into core with a listing of the options such as "LIST," "SAVE," "RUN" or "EXIT" to be displayed on the CRT. "LIST" would list all of the variables for that program. Upon selecting a variable with cursor, a description of the variable would be displayed and a buffer into which a new value could be written would be available. The executive would permit the programs to be accessed, varied and executed in any order desired.

IMAGE CALCULATION AND DISPLAY SYSTEM

The system would allow a series of programs to be interactive. A program PLOT will be written which will allow a model for the structure of the material to be plotted along any desired direction. The cross-hair cursor would enable an atom to be deleted, inserted or moved to any position and the resulting coordinates would be input into program FCOEFF which calculates the Fourier coefficients for that structure. Program DEFECT would then be loaded and an image for the structure would be calculated and displayed. At this point the image could be saved on magnetic tape or deleted and recalculated with different values of the image parameters. Alternatively the structural model could be changed (by returning to program PLOT) and programs FCOEFF and DEFECT rerun to yield an image. The data for all of the calculations will be stored in common so that it will be unnecessary to load them for every program. By this procedure the effect on the image of a displacement of one or several atoms could be rapidly determined.

Other programs useful for electron diffraction and imaging such as INTPLT which plots the characteristics of the diffracted beams or DIFPLT which plots X-ray or electron diffraction patterns could be executed on this system with their output displayed on the CRT.

Future Plans

The immediate goal is to have a functioning image calculation system to perform rapid calculations and graphical displays of electron images. With the AD-1 area scan program it would be possible to digitize the experimental electron micrographs and display them also on the CRT. A disc operating system would be required to actually perform image enhancement using the computer because of the large amount of points required. It would however be possible to digitize the experimental image onto magnetic tape, process it on the UNIVAC 1110, write it back on tape and then display it on the graphics terminal. It is possible that a split screen with the experimental image on one side and the calculated image on the other could be used to improve visual comparison. It is also feasible that a difference image could be calculated by a numerical point-to-point comparison and the resulting image displayed on the CRT.

REFERENCES

1. P. Kunzmann and L. Eyring, J. Solid State Chem., 14, 229-237 (1975).

2. A. J. Skarnulis, Ph.D. Dissertation, 1976, Arizona State University.

IV

SINGLE CRYSTAL STUDIES
OF FLUORITE-RELATED
INTERMEDIATE PRASEODYMIUM OXIDES

INTRODUCTION

The growth of high quality single crystals of members of the homologous series of praseodymium oxides is essential before a structural investigation by X-ray or neutron diffraction can be initiated. Several years ago a method was developed to grow single crystals of PrO_2 using hydrothermal techniques. By providing suitable oxygen activity and temperature, earlier attempts to adjust the composition of these crystals packed in large amounts of powder were discouraging. The crystals were highly defective showing sufficient twinning and disorder to make them useless for single crystal diffraction work.

Recently, however, some preparations of intermediate phases using a microbalance to monitor the composition of crystals in the absence of powder was apparently successful. (It had in the meantime been observed that there is a shift in the (P, X, T) curve for the single crystals compared to the powder.) At present two different members of the homologous series consisting of a single orientation have been obtained. A discussion of the preparation procedures and the ensuing single crystal diffraction studies on these specimens follows.

EXPERIMENTAL

Preparation

Suitable single crystals of PrO_2 were prepared hydrothermally as previously described.[1] These crystals consisted of some well-formed irregular octahedra from 0.1 to 0.7 mm across and mixed in with other ill-defined crystals of similar size. A 0.5 g sample of this material was introduced into the Cahn thermogravimetric balance[2] which was then evavacuated. The oxygen pressure was adjusted to 10 Torr at room temperature. The conditions were changed stepwise to 10 Torr O_2 and 565°C to reduce the crystals to the composition $PrO_{1.778}$ (Zeta phase). The reduction was followed by the change in mass of the sample on the balance. It is interesting that these conditions are at the upper end of the stability range found for the zeta phase for a powder sample.[3] After the sample had reached the proper composition it was annealed at these conditions for ten days.

Investigation by oscillation X-ray photographs and the autodiffractometer indicated that many of these crystals were single phase $PrO_{1.778}$ and showed little evidence of twinning or disorder. The crystals were then divided into three batches which were wrapped in platinum foil and sealed in quartz ampules at sufficient oxygen pressure so that the conditions of the original reduction would be maintained when heated. The three samples were allowed to anneal at 565°C and 10 Torr O_2, one for 30 days, the second for 150 days and the third is still in the furnace. Each tube was taken from the furnace and rapidly cooled in cold water. The crystals were then kept in a dry atmosphere to prevent decomposition. Investigation of crystals from both annealing batches by oscillation photographs and/or the autodiffractometer indicated these crystals were also single phase and untwinned but were of the $PrO_{1.800}$ (epsilon) phase.

X-Ray Diffraction Studies--Zeta Phase

A number of single crystals of $PrO_{1.778}$ were investigated by oscillation photography using Zr filtered $MoK\alpha$

radiation. These crystals were mounted on glass fibers and coated with several layers of shellac in an attempt to protect them from the atmosphere. From the sharpness and extent of the superlattice reflections one individual was selected for further investigation on the Syntex $P\bar{1}$ Autodiffractometer. A series of reciprocal lattice scans showed no evidence of twinning and indicated that the crystal was single phase. Unfortunately, during this examination a rapid deterioration of the crystal was evident, probably by reaction with the atmosphere, despite the protective coating. As the remaining crystals were being annealed further we could not examine another crystal of the original material.

Epsilon Phase

This investigation proceeded in much the same way as for the zeta phase crystals except that these crystals were placed in glass capillaries which were sealed to prevent reaction with the atmosphere. Crystals protected in this way show no evidence of decomposition. A number of these crystals from both annealing batches were investigated by oscillation photography. A well-formed individual displayed a five-times superlattice spacing of sharp reflections along the fluorite

(011) direction which is compatible only with the lattice parameters of the epsilon phase. Subsequent investigation on the diffractometer confirmed this observation. This crystal has the appearance of a truncated tetrahedron approximately 0.12 mm thick and 0.28 mm across the base. A refinement of the setting angles for fifteen fluorite-related reflections within the range $12.9° \leq 2\theta \leq 25.0°$ gave the lattice parameters $\underline{a} = 6.728(4)$, $\underline{b} = 19.319(12)$, $\underline{c} = 15.480(10)$ Å, $\beta = 125.46(4)°$ which confirm the choice of unit cell obtained from electron diffraction photographs.[4] A more convenient unit cell was later chosen and has the lattice parameters $\underline{a} = 6.728$, $\underline{b} = 19.319$, $\underline{c} = 12.800$ Å, and $\beta = 100.19°$. A total of 9895 reflections of indices $(\pm h, \pm k, \pm \ell)$ was collected using graphite monochromated $MoK\alpha$ radiation ($2\theta \leq 60.0°$) in the θ-2θ scan mode at a scan rate of $1°$ min^{-1} on 2θ. The scan range was from $2\theta K\alpha_1 - 0.7°$ to $2\theta K\alpha_2 + 0.7°$ with a background count of 0.25 of the scan time taken at each end of the scan.

Three standard reflections including one superlattice reflection were periodically monitored and showed a maximum 5% fluctuation during the data collection. The intensities were corrected for Lorentz and polarization effects for monochromated radiation[5] and an analytic absorption correction[6] was applied for $\mu = 350.5\ cm^{-5}$.

It was evident from the symmetry of the intensity data and the refined values of the lattice parameters that the Laué symmetry of the crystal was 2/m and consequently the corrected structure factors were merged[7] to give 4633 nonzero reflections. The residual, $R = \frac{\Sigma \left| F_1 \right| - \left| F_2 \right|}{\Sigma \left| \overline{F} \right|}$, for the merged data set was 0.109. In addition, the pattern of extinctions appeared to be $h0\ell$, $\ell = 2n+1$ and $0k0$, $k = 2n+1$ which conforms to the space group $\underline{P2_1/c}$. This was further confirmed by an N(z) test[8] on the superlattice reflections which indicated a centrosymmetric intensity distribution.

Structure Analysis

A set of idealized coordinates based on the fluorite substructure was developed for the second choice of unit cell in the space group $\underline{P2_1/c}$; these coordinates are listed in Table I. The unit cell contents of such a set of sites is $Pr_{40}O_{80}$, hence two of these oxygen positions must be vacant to give the epsilon phase composition of $Pr_{40}O_{72}$ per unit cell. These 20 available unique oxygen positions allow for 190 combinations of two oxygen vacancy positions. This long list was reduced to eight unique and chemically plausible models for the vacancy positions which are listed in Table II. The other models were rejected because they either were related to the unique set by origin shifts or centering operations, or had a symmetry higher than $\underline{P2_1/c}$. The chemical restriction that no two vacancies could be adjacent was also applied to the set of models.

Each of these models was tested in a least-squares refinement of the metal positions using the 3173 largest reflections. In each case the four metal atoms surrounding each vacancy position were displaced ~ 0.17Å away from the vacancy to conform with the results of the neutron diffraction study of Pr_7O_{12}[9] and to break the pseudofluorite symmetry of the ideal positions. Each reflection was assigned a weight, $w = (|F_0|/500)^2$ for $|F_0| < 500$, or a weight, $w = (500/|F_0|)^2$ for $|F_0| > 500$; there were 152 reflections with $|F_0| > 500$ and 3021 with $|F_0| < 500$. From 3 to 6 cycles of least-squares were required to obtain reasonable convergence with the residuals shown in Table III.

From these results it is clear that model 5 is inferior to the rest of the possible models and that to distinguish among the others a more complete refinement is necessary. This work is currently in progress.

REFERENCES

1. M. Z. Lowenstein, L. Kihlborg, K. H. Lau, J. M. Haschke and L. Eyring, NBS Spec. Publ., 364, 343 (1972).

2. A. T. Lowe and L. Eyring, J. Solid State Chem., 14, 383 (1975).

3. B. G. Hyde, D. J. M. Bevan and L. Eyring, Phil. Trans. Roy. Soc., Series A, 259, 583 (1966).

4. P. Kunzmann and L. Eyring, J. Solid State Chem., 14, 229 (1975).

5. L. V. Azaroff, Acta Cryst., 8, 701 (1955).

6. A revised version of the Alcock analytical absorption program was used in this analysis.

7. All calculations other than data reduction and absorption corrections were done using the CRYSTALS computing package: R. S. Rollett and J. R. Carruthers, personal communication.

8. E. R. Howells, D. C. Phillips and D. Rogers, Acta Cryst., 3, 210 (1950).

9. R. B. Von Dreele, L. Eyring, A. L. Bowman and J. L. Yarnell, Acta Cryst., B31, 971 (1975).

TABLE I

Idealized Atomic Positions for Epsilon Phase

Atom	x	y	x
Pr 1	0	0	0
Pr 2	.5	0	.5
Pr 3	.75	0	.25
Pr 4	0	.4	0
Pr 5	0	.3	.5
Pr 6	.5	.2	.5
Pr 7	.5	.1	0
Pr 8	.25	.1	.25
Pr 9	.25	.3	.25
Pr 10	.75	.4	.25
Pr 11	.75	.2	.25
O 1	.0625	0	.1875
O 2	.1875	.5	.0625
O 3	.3125	.5	.4375
O 4	.4375	0	.3125
O 5	.0625	.4	.1875
O 6	.1875	.1	.0625
O 7	.3125	.1	.4375
O 8	.4375	.4	.3125
O 9	.5625	.1	.1875
O 10	.6875	.4	.0625
O 11	.8125	.4	.4375
O 12	.9375	.1	.3125
O 13	.0625	.2	.1875
O 14	.1875	.3	.0625
O 15	.3125	.3	.4375
O 16	.4375	.2	.3125
O 17	.5625	.3	.1875
O 18	.6875	.2	.0625
O 19	.8125	.2	.4375
O 20	.9375	.3	.3125

TABLE II

Possible Vacancy Positions for Epsilon Phase

Model	Atom	Ideal Vacancy Position x	y	z
1	O 1	.0625	0	.1875
	O 14	.1875	.3	.0625
2	O 1	.0625	0	.1875
	O 15	.3125	.3	.4375
3	O 1	.0625	0	.1875
	O 16	.4375	.2	.3125
4	O 5	.0625	.4	.1875
	O 16	.4375	.2	.3125
5	O 9	.5625	.1	.1875
	O 10	.6875	.4	.0625
6	O 9	.5625	.1	.1875
	O 14	.1875	.3	.0625
7	O 11	.8125	.4	.4375
	O 14	.1875	.3	.0625
8	O 11	.8125	.4	.4375
	O 16	.4375	.2	.3125

TABLE III

Residuals for the Refinement of the Metal Atom Positions in the Epsilon Phase Models

Model	R	R_w [a]
1	38.32	21.02
2	41.24	21.24
3	41.31	22.03
4	37.12	20.13
5	49.93	24.83
6	41.54	21.79
7	37.19	20.35
8	41.83	22.68

[a] $R_w = (\Sigma w(|F_0| - |F_c|)^2 / \Sigma w |F_0|^2)^{\frac{1}{2}}$

V

AN ELECTRON MICROSCOPIC STUDY OF EPSILON PHASE ($Pr_{10}O_{18}$)

Crystals of the phase $Pr_{10}O_{18}$ obtained from the same preparation that yielded the single crystals for the X-ray investigation were ground under liquid nitrogen and examined in a high resolution electron microscope. A crystal structure image from a $\langle 100 \rangle_{10}$ ($\equiv \langle 21\bar{1} \rangle_F$) zone of epsilon is shown in Figure 1. A periodic rectangular array of bright spots of dimension $\sim$ 19Å x $\sim$ 12.5Å corresponding to the projection of the unit cell in this direction can be readily discerned. Additional contrast is apparent within the unit cell exhibiting a rather complicated pattern of spots which doesn't appear to be completely resolved.

Currently programs FCOEFF and DEFECT are being used to calculate crystal structure images for the eight possible structural models for the $\underline{P2_1/c}$ symmetry of epsilon. For each model tested the input metal positions obtained are those obtained from the least-squares refinement of the single crystal X-ray data and the oxygen positions are the ideal fluorite positions. Calculated crystal structure images at various defocus values for one of the proposed structural models for epsilon phase (model 1, oxygen vacancies O1 ' and O14) are displayed in Figure 2. These images were calculated for crystals 148Å thick which is thought to be approximately the thickness of the thinnest fragments examined in the microscope. The arrangement of the spot array in several of these calculated patterns has some resemblance to the observed image, however, it is not possible to conclusively say that this model represents the structure of epsilon. In order to obtain a more accurate comparison between the calculated and experimental images a through-focus series needs to be taken on the electron microscope. Also, further calculations at different crystal thicknesses with the inclusion of convergence of the beams are required. This work is presently in progress.

FIGURE LEGENDS

1. Observed crystal structure image from a $\langle 100 \rangle_{10}$ zone of epsilon.

2. Calculated $\langle 100 \rangle_{10}$ crystal structure images of $Pr_{10}O_{18}$ showing variation with defect of focus for a crystal thickness of 148Å.

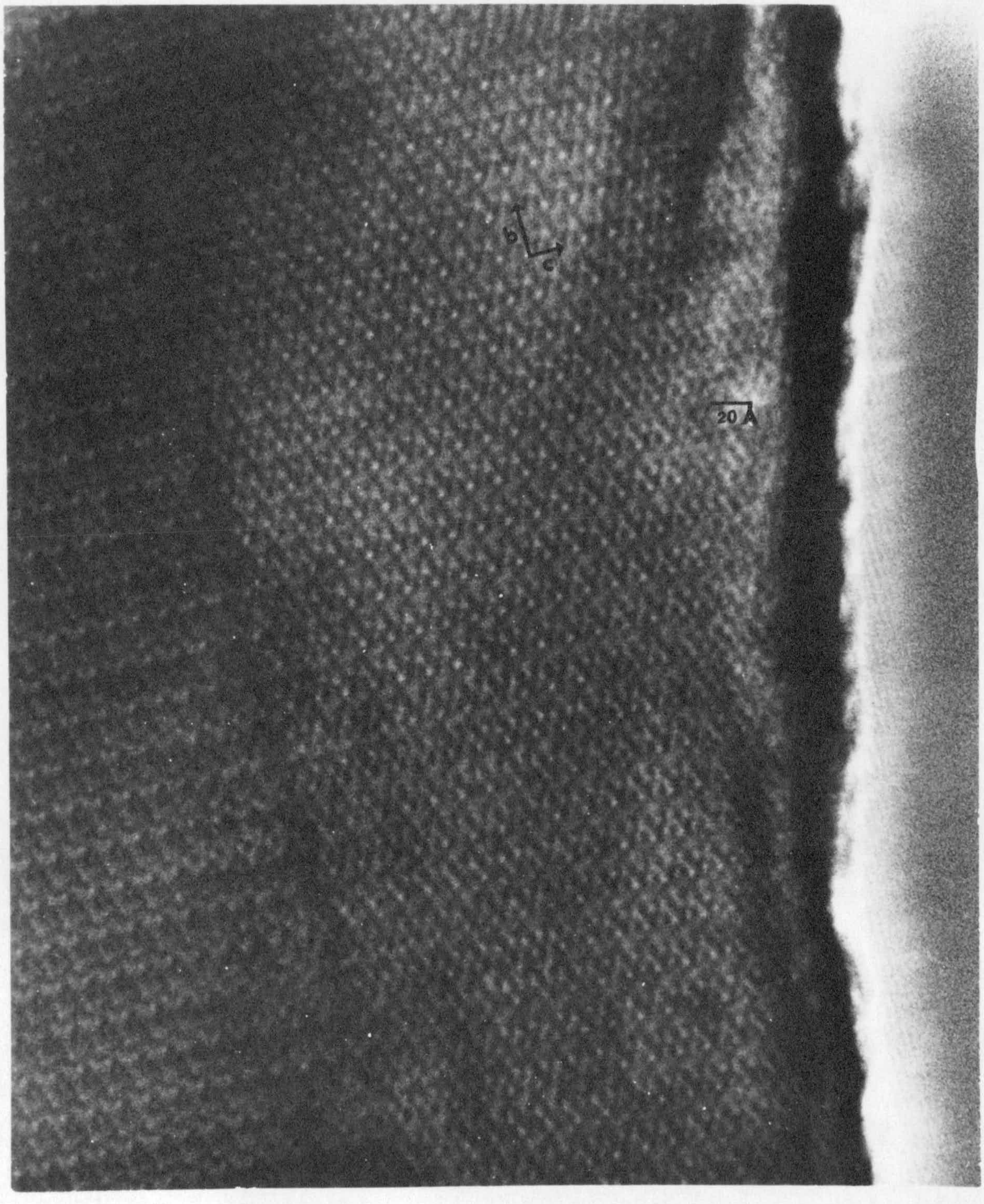

Figure 1. Observed crystal structure image from a $\langle 100 \rangle_{10}$ zone of Epsilon.

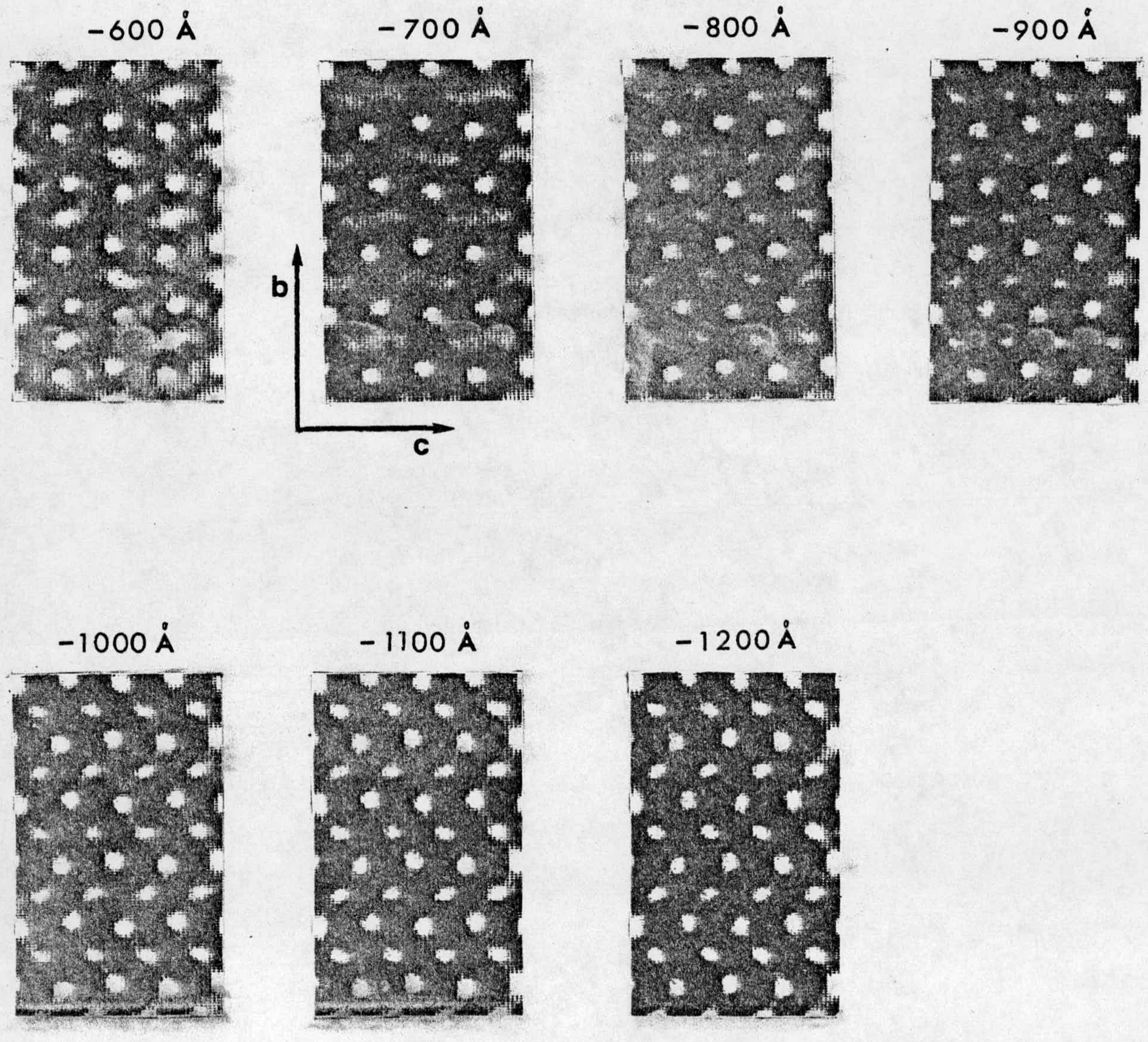

Figure 2. Calculated $\langle 100 \rangle_{10}$ crystal structure images of $Pr_{10}O_{18}$ showing variation with defect of focus for a crystal thickness of 148Å.

VI

A STUDY OF ORDERING IN THE $Er_2O_3 \cdot xHfO_2$ SYSTEM

The ceramics group at the Ames Laboratory of ERDA has been studying the properties of ternary ceramics composed of hafnia and the rare earth oxides. We have begun to look at some of their specimens.

Dr. M. Berard has supplied us with sintered specimens of the following composition and grain size.

Composition	Grain Size
1. 100% Er_2O_3	50.70 μm
2. 90 mole% Er_2O_3 -10 mole% HfO_2	~ 25 μm
3. *$33\frac{1}{3}$ mole% Er_2O_3 -$66\frac{2}{3}$ mole% HfO_2	~ 20 μm
4. 20 mole% Er_2O_3 -80 mole% HfO_2	~ 20 μm

Samples 1 - 4 were sintered in vacuum for eight hours at 2000°C followed by reoxidation for 14 hours at 1200°C in air. * Part of Sample 3 was annealed for a much longer time to promote ordering.

These samples were ground in a mortar and pestle under liquid nitrogen (a technique known to give thinner crystals in the rare earth oxides) and the crystal fragments introduced onto a microscope grid to which a holey carbon film had been applied.

Some preliminary observations have been made. The electron diffraction patterns of Samples 1 and 2 indicated well-crystallized C-type cubic structures indicating the range of composition of this phase at least to 10 mole % HfO_2. Electron diffraction patterns of Specimens 3 and 4 as well as the long-time anneal of 3 showed marked diffuse scatter about the strong fluorite spots. Figure 1 compares samples containing 90% Er_2O_3 and $33\frac{1}{3}$% Er_2O_3 in the $[21\bar{1}]_F$ and $[111]_F$ zones. The bright spots are those due to the fluorite-related sub-structures. The crystals did not give images showing good detail and have not been interpreted.

Allpress and Rossell[1] have done a corresponding electron microscopic study of the calcia-hafnia system and have found diffuse scatter remarkably similar to that shown in Figure 1 for incompletely annealed samples. In this case, however, the diffuse rings apparent in the $[21\bar{1}]$ zone (Figure 1) are relatively much smaller, being about 1/6 or 1/7 the spacing of the main fluorite reflections, whereas in the case of the calcia-hafnia system they are about 1/4.

The calcia-hafnia results were interpreted as suggesting that the solid solutions contained domains of the Φ_1 phase, $CaHf_4O_9$, embedded coherently in a number of specific orientations within the fluorite matrix. The domains were estimated to be about 30 Å in diameter based on calculations from such a model.

This work will be carried forward in an effort to clarify ordering in this ternary system. In the process the credibility of the model of Allpress and Rossell will be tested and more learned about how defects are accommodated in fluorite-related oxides. If the model is correct the intergrown phase in the $Er_2O_3 \cdot HfO_2$ system is certainly a different one than Φ_1. There are many possibilities. It would be desirable to anneal the specimen longer in an effort to obtain the intergrown phase in sufficiently large crystal size to observe the pattern of the ordered phase.

REFERENCES

1. J. G. Allpress and H. J. Rossell, J. Solid State Chem., 15, 68 (1975).

FIGURE LEGENDS

1. Electron Diffraction Patterns of Phases in Erbia-Hafnia Ceramics a) the $[111]_F$ zone, b) the $[21\bar{1}]_F$ zone.

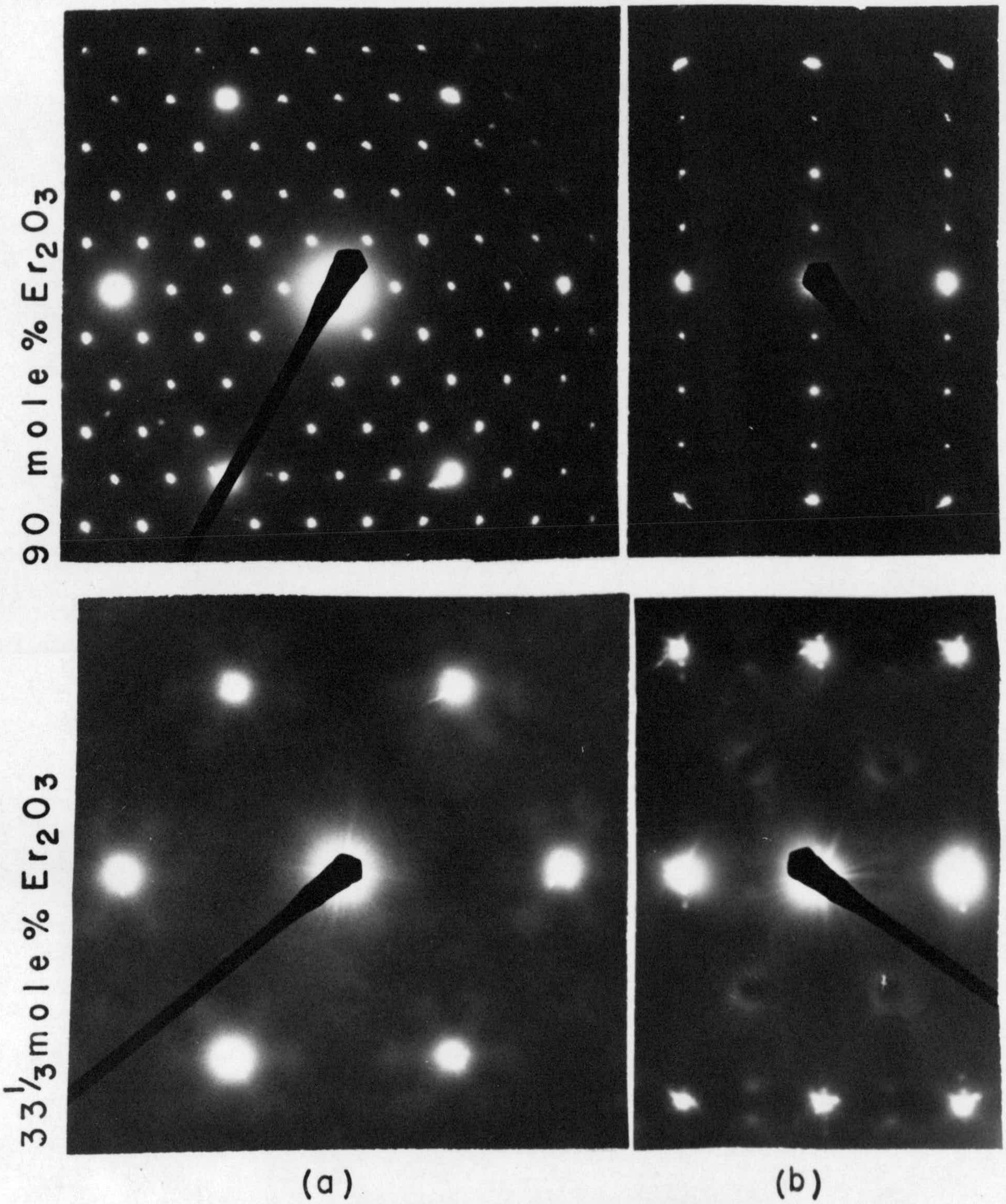

Figure 1. Electron Diffraction Patterns of Phases in Erbia-Hafnia Ceramics a) the $[111]_F$ zone, b) the $[21\bar{1}]_F$ zone.